ent ages due to the higher capacity for megakaryopoiesis in *Lnk*$^{-/-}$ animals after BM transplantation. However, using intravital microscopy after laser-induced injury, we were able to compare thrombus formation in *Lnk*$^{-/-}$ and WT mice of the same age and show that thrombus formation is impaired in *Lnk*$^{-/-}$ animals despite higher numbers of circulating platelets (Figure 3, C and D). The reduced thrombus formation by Lnk-deficient platelets was even apparent 4 weeks after transplantation, at which time chimeric mice show slight thrombocytopenia, reflecting the fact that they are recovering from severe myelosuppression, and so are actively generating platelets. Furthermore, our in vitro study of the spreading of platelets from chimeric mice of different ages confirmed that the area of spread of platelets from Lnk-chimeras was consistently smaller than the area of spread of platelets from WT-chimeras. From these findings, we again conclude that Lnk deficiency leads to impaired platelet spreading independent of age or active megakaryopoiesis and contributes to the impaired stabilization of developing thrombi in vivo.

The small GTPase Rac1 and its guanosine exchange factor Vav contribute to the formation of lamellipodia during the adhesion of CHO-αIIbβ3 cells to fibrinogen (29, 37). The activation of Rac1 is mediated through 2 NxxY motifs (residues 744–747 and 756–759 in the β3 subunit) in the cytoplasmic tail of the β3 subunit (37). Reddy et al. recently demonstrated that CHO cells expressing a truncated form of αIIbβ3 lacking the distal NxxY motif (residues 756–759) fail to spread on fibrinogen, and the defect is rescued by overexpression of active Fyn (20). Those results indicate that Fyn activation may augment functions of the proximal NxxY motif (residues 744–747), presumably through phosphorylation of Tyr747 (8). Our results support that idea and indicate that Fyn, with the help of Lnk, is required for Tyr747 phosphorylation of β3 (Figure 6, A and B). In the model cell system, Lnk was directly tyrosine phosphorylated at Tyr536 by c-Src, which was required for formation of lamellipodia by CHO-αIIbβ3 cells immobilized on fibrinogen (Supplemental Figure 5). Because Lnk supports Fyn's association with the αIIbβ3 complex but is not required for c-Src activation or its association with the αIIbβ3 complex in platelets (Figure 6A), we propose the signaling cascade depicted in Figure 7. The Fyn binding region of β3 — residues 721–725 (IHDRK) (20) — is distinct from the c-Src binding region — residues 760–762 (RGT) (38). In normal platelets, the engagement of integrin αIIbβ3 initiates outside-in signaling through c-Src activation and Syk recruitment to the β3 tail (4, 5, 31), which is independent of Lnk. The activated c-Src presumably mediates tyrosine phosphorylation of Lnk, which leads to efficient recruitment/activation of Fyn at the β3 tail and phosphorylation of Tyr747 (Figure 7). We studied the effects of CVX on inside-out signaling by measuring fibrinogen binding to integrin αIIbβ3 and on outside-in signaling by studying platelet spreading on a collagen-coated surface (data not shown). The results so far indicate that Lnk is not involved in signaling mediated through GPVI, where Fyn also functions, and it appears that Lnk deficiency does not universally affect Fyn-coupled platelet receptors. Although the precise molecular mechanism is currently unknown, presumably the necessary machinery exists to ensure the specific and selective interaction of Lnk and the Fyn complex with the β3 integrin subunit.

It has been reported that the laser-induced injury model mainly reflects the tissue factor/thrombin–mediated pathway to platelet activation and is independent of the exposed collagen-GPVI and vWF-GPIbα interactions triggered by the loss of endothelium; conversely, $FeCl_3$-induced thrombus formation is collagen and vWF dependent (23, 25, 39). Nonetheless, it is reasonable to consider that our laser-induced injury model caused relatively mild damage to endothelial cells, as compared with previously reported experimental models (26). Consistent with that idea, we found that staining of the vasculature for *Griffonia simplicifolia* IB_4 isolectin showed the endothelial layer to be intact after laser-induced injury (Supplemental Figure 7). In addition, there was no extravasation of fluorescent dyes after laser injury, indicating that vascular permeability was unaffected by laser-induced injury (Supplemental Videos 1–8). Although, as with other methods, the precise mechanism and trigger of laser-induced thrombus formation remain unclear, it is unlikely that exposure of the extracellular matrix (mainly collagen) as a result of endothelial damage is a primary trigger. One alternative possibility is that thrombus formation is triggered by ROS, but ROS produced within the blood as a result of laser irradiation of hematoporphyrin and fluorescent dyes are readily washed away by the rapid blood flow. More likely, ROS produced within endothelial cells and/or stromal spaces are involved.

Given the mild damage to the endothelium and the lack of involvement of the collagen-GPVI and vWF-GPIbα interactions, the diminished thrombus formation seen in *Lnk*$^{-/-}$ platelets could reflect a defect in αIIbβ3-mediated signaling. Recently, 2 distinct phases in the stabilization of the primary hemostatic plug under flow conditions have been proposed. The first is a rapid phase linked to fibrin-independent platelet contractility (40), possibly accomplished through αIIbβ3-mediated outside-in signaling and the subsequent Rho kinase–dependent physical tightening of platelet-platelet adhesion contacts, for example, through ephrin/Eph kinases, JAM-A, or Sema4D (41). The second is a slower phase linked to thrombin generation and fibrin polymerization to stabilize the thrombus (40).

With our imaging system and laser-induced injury, we were able to observe the rapid phase of thrombus formation, which occurs within seconds, whereas $FeCl_3$-induced arterial occlusion occurs more than 20 minutes after injury. Using chimeric mice in which platelet counts were equalized, we observed that in vivo thrombus formation by *Lnk*$^{-/-}$ platelets was impaired in both models, although more significant deficiencies were detected in the laser-injury model (Figure 2C and Figure 3A).

Recent genome-wide association studies identified SNPs associated with type 1 diabetes and celiac disease, including a nonsynonymous SNP in exon 3 of LNK/SH2B3, encoding a pleckstrin homology domain (R262W) (42, 43). Notably, the same SNP was recently shown to be associated with increased eosinophil numbers and myocardial infarction (42, 43). Accordingly, it will be important to investigate the link between the sequence variation in LNK/SH2B3 and platelet function in patients.

In conclusion, we explored a new regulatory mechanism by which the adaptor protein Lnk contributes to the stabilization of developing thrombi. Lnk regulates integrin αIIbβ3–mediated signaling in platelets and is required for Fyn interaction with αIIbβ3 and efficient tyrosine phosphorylation of the β3 integrin subunit, leading to actin cytoskeletal reorganization. Because *Lnk*$^{-/-}$ mice do not exhibit spontaneous (or abnormal) bleeding or severe immune system dysfunction, we suggest that molecules that modulate outside-in signaling, including Lnk, might represent novel and safe therapeutic targets for the prevention of cardiovascular events. Such therapeutics would likely pose a smaller risk for bleeding than conventional drugs.

Methods

Cells, reagents, and mice. All reagents were from Sigma-Aldrich unless otherwise indicated. C57BL/6 mice congenic for the Ly5 locus (B6-Ly5.1) and *Lnk*$^{-/-}$ B6-Ly5.1 mice (22) were bred and maintained at the Animal Research Centers of the Institute of Medical Science, the University of Tokyo, and of the Research Institute, International Medical Center of Japan. *Lnk*$^{-/-}$ B6-Ly5.1 mice were first established on a C57BL/6 (B6-Ly5.2) background and backcrossed more than 12 times, after which they were crossed into the B6-Ly5.1 background. WT B6-Ly5.2 mice were purchased from Nihon SLC. *Fyn*$^{-/-}$ B6-Ly5.2 mice (44) were from T. Yamamoto (University of Tokyo). The protocol for this work was approved by the IACUCs of the Institute of Medical Science, University of Tokyo, and of the Research Institute, International Medical Center of Japan. The following Abs and reagents were used: anti-c-Src (327, a gift from J. Brugge, Harvard Medical School, Boston, Massachusetts, USA) (4, 31), anti-mouse αIIbβ3 (1B5, from B. Coller, Rockefeller University, New York, New York, USA), anti-human Lnk (from J. Hayashi, University of Maryland, Baltimore, Maryland, USA, or purchased from Abcam), anti-mouse Lnk (11), anti-Lcp2 and anti-Fyb (from G. Koretzky, University of Pennsylvania, Philadelphia, USA), anti-phospho-Src pY418 and anti-phospho-β3 pY773 (Y747 in mice) (Biosource International), anti-Syk (N-19), anti-Fyn (FYN3) and anti-β3 integrin (N-20) (Santa Cruz Biotechnology Inc.), anti-phosphotyrosine (4G10) and anti-Src (GD11) (Upstate Biochemical), anti-Fyb and anti-αIIb (MWReg30, BD Biosciences and Invitrogen), HRP-conjugated secondary Abs (Bio-Rad), Protein G Sepharose (GE Healthcare), protease inhibitor cocktail, aprotinin, and leupeptin (Roche Molecular Biochemicals), rhodamine-phalloidin, Alexa Fluor 488–conjugated fibrinogen, and Alexa Fluor 488–conjugated bovine IgG Abs (Molecular Probes, Invitrogen), purified human fibrinogen (American Diagnostica Inc), FITC-conjugated anti-mouse integrin α2, αIIb, and β3 and the FITC-Annexin-V kit (BD and Invitrogen), PE–anti-mouse GPIbα, FITC–anti-mouse GPVI, and PE–anti-mouse P-selectin (Emfret), and CVX (from T. Morita, Meiji Pharmaceutical University, Tokyo, Japan).

BM transplantation. BM from femurs was washed with PBS and counted. WT (10^7 per recipient mouse) or *Lnk*$^{-/-}$ (2×10^5 or 5×10^5) BM cells were intravenously transfused into 8-week-old male Ly-5.2 recipient mice. The recipients were then lethally irradiated at a dose of 9.5 Gy. Two, 4, 6, and 8 weeks later, PBLs were collected from the recipient mice, and chimerism was confirmed using a Ly5.1/Ly5.2 system.

Bleeding times. Tail bleeding assays were performed with 8- to 12-week-old *Lnk*$^{-/-}$ and WT male mice. Mice were anesthetized with 50 μg/ml pentobarbital, after which a 5-mm segment of the distal tip of the tail was cut off, and the tail was immediately immersed in PBS at 37°C. Tail bleeding times were defined as the time required for the bleeding to stop. Tail bleeding was monitored for at least an additional 60 seconds to detect possible re-bleeding (secondary bleeding), as previously described (8, 20, 45). We preliminarily confirmed that tail bleeding and re-bleeding times were comparable in B6-Ly5.1 and B6-Ly5.2 mice.

Measurement of $FeCl_3$-induced vessel occlusion times in carotid arteries. Mice were anesthetized by injection with urethane (1.5 g/kg), and a segment of the carotid artery was exposed. Thrombus formation was then triggered by applying 10% $FeCl_3$ solution to the adventitial side to induce endothelial cell injury (23). FITC-dextran solution (5 mg/kg BW, MW 150,000) was injected via the tail vein, and carotid blood flow was continuously monitored using fluorescence confocal microscopy to determine the time to occlusion.

Intravital microscopy and thrombus formation. To visually analyze thrombus formation in the microcirculation of the mesentery in living animals, we used in vivo laser injury and visualization techniques developed through modification of conventional methods (18, 24). Male mice were anesthetized by injection with urethane (1.5 g/kg), and a small incision was made so that the mesentery could be observed without being exteriorized. FITC-dextran (5 mg/kg BW) was injected into mice to visualize cell dynamics, while hematoporphyrin (1.8 mg/kg for capillary thrombi, 2.5 mg/kg for arterioles) was injected to produce ROS upon laser irradiation. Blood cell dynamics and production of thrombi were visualized during laser excitation (λ 488 nm, 30 mW power). Sequential images were obtained for 20 seconds at 30 frames/s using a spinning-disk confocal microscope (CSU22, Yokogawa Electronics) and an EM-CCD camera (Impactron CCD; Nihon TI). The diameters of the examined capillaries were as follows: in Figure 3A, WT-chimera 6.56 ± 0.12 μm, Lnk-chimera 6.68 ± 0.06 μm (n = 30 vessels from 5 animals, P = 0.42); in Figure 3C, *Lnk*$^{-/-}$ 6.56 ± 0.12 μm, WT 6.46 ± 0.10 μm, *Lnk*$^{-/-}$ 6.56 ± 0.12 μm (n = 30 vessels from 5 animals, P = 0.26). In Figure 3D, diameters of the examined arterioles were as follows: WT 26.6 ± 4.5 μm, *Lnk*$^{-/-}$ 25.7 ± 3.4 μm (n = 10 vessels from 5 animals, P = 0.43). We also confirmed that thrombus formation within the vessels was comparable in the B6-Ly5.1 and B6-Ly5.2 mice.

Preparation of blood samples for analysis of platelet spreading and fibrinogen binding. For each experiment, blood samples were collected from 8–10 *Lnk*$^{-/-}$ and WT male mice (8–12 weeks old) by cardiac puncture after CO_2 treatment. Some collected samples were immediately transferred to plastic tubes containing one-sixth volume of acid-citrate-dextrose (ACD). Platelet-rich plasma (PRP) was obtained by centrifugation of whole blood at 150 *g* for 15 minutes without braking. To obtain the washed platelets used for most of the in vitro experiments, 1 μM PGE_1 and 2 U/ml apyrase were added, and the platelets were centrifuged at 750 *g* for 10 minutes. The sedimented platelets were then washed in modified Tyrode-HEPES buffer containing 1 μM PGE_1 plus 15% volume ACD and finally resuspended in an appropriate volume of Ca^{2+}-free modified Tyrode-HEPES buffer (10 mM HEPES [pH 7.4], 12 mM $NaHCO_3$, 138 mM NaCl, 5.5 mM glucose, 2.9 mM KCl, and 1 mM $MgCl_2$).

Confocal microscopic analysis of platelet spreading and immunoprecipitation assays. All confocal studies were performed using a Leica TCS SP2 microscope equipped with a 63×, 1.40 NA oil immersion objective (Leica), as described previously (46). Images were assembled using Adobe Photoshop. Analysis of platelet adhesion (cell number) and calculation of their surface area (spreading) were done using NIH ImageJ software (http://rsbweb.nih.gov/ij/).

The lysis buffer used for immunoprecipitation contained 2% Triton X-100 or 1% NP-40, 150 mM NaCl, 50 mM Tris-HCl (pH 7.4), 0.5 mM EGTA, 0.5 mM EDTA, 1 mM Na_3VO_4, 0.5 mM NaF, 0.5 mM PMSF, and 50 μg/ml leupeptin. Anti-αIIb was used for immunoprecipitation of αIIbβ3.

Flow cytometric measurement of fibrinogen-binding (activation of αIIbβ3) and P-selectin expression. Washed, rested platelets were incubated for 30 minutes at room temperature with 200 μg/ml Alexa Fluor 488–conjugated fibrinogen plus ADP, epinephrine, PAR4 agonist peptide, or PMA in a 50-μl final volume of modified Tyrode-HEPES buffer containing 0.2 mM $CaCl_2$. The binding of Alexa Flour 488–fibrinogen to platelets was quantified using an Aria flow cytometer (BD). Nonspecific binding was determined in the presence of 20 μg/ml 1B5. Specific binding was defined as total minus the nonspecific binding. P-selectin expression was measured similarly using a Canto-II flow cytometer (BD) with washed platelets in a 100-μl final volume (1×10^6 platelets).

Clot retraction assay. To obtain washed platelets, PRP from WT or *Lnk*$^{-/-}$ mice was diluted with 1 volume of modified Tyrode-HEPES buffer and centrifuged in the presence of 0.15 μM PGE_1. The sedimented platelets were then washed in modified Tyrode-HEPES buffer containing 0.15 μM PGE_1 and 1 mM EDTA and finally resuspended with modified Tyrode-HEPES buffer to adjust the number of platelets to 3×10^8/ml. Fibrin clot retraction was studied by incubating the clots in the presence of 2 U/ml

thrombin, 500 μg/ml fibrinogen, and 2 mM $CaCl_2$ for 1 or 2 hours at 37°C in an aggregometer cuvette as described previously (47, 48).

Plasmids and transfection of COS7 or CHO cells. COS7 and CHO-αIIbβ3 cells (provided by H. Kashiwagi, Osaka University, Osaka, Japan) were transfected using Lipofectamine 2000 methodology (Invitrogen). Constitutively active human c-Src mutant (Y530F)/pcDNA3 was obtained from T. Tezuka (University of Tokyo). Flag-tagged Lnk and the C-terminal deletion mutant (ΔC-Lnk) were constructed by PCR using previously constructed plasmids (34) as templates and reinserted into pcDNA3 vector. A Lnk cDNA cassette lacking the stop codon was generated by PCR and inserted into pcDNA-DEST47 (Invitrogen) to generate the expression vector for the Lnk-GFP fusion protein, as described previously (34).

Statistics. Differences between experimental and control animals were analyzed using 2-tailed Student's *t* tests. Incidence of re-bleeding times was evaluated by the χ^2 test. *P* values less than 0.05 were considered significant.

Acknowledgments

The authors thank J. Brugge, B. Coller, J. Hayashi, H. Kashiwagi, G. Koretzky, T. Morita, and T. Tezuka for providing reagents or cells and T. Yamamoto for *Fyn*-null mice. We are also grateful to J. Seita, H. Tsukui, A. Yamasaki, K. Wakabayashi, and M. Tajima for their excellent technical help. This work was supported by Grants-in-Aid and Special Coordination Funds for Promoting Science and Technology from the Ministry of Education, Culture, Sports, Science and Technology and from the Ministry of Health, Labour and Welfare, by the Japanese Sharyou Foundation (Tokyo, Japan), by the Uehara Memorial Foundation (Tokyo, Japan), and by the Mitsubishi Pharma Research Foundation (Osaka, Japan). H. Takizawa and S. Nishimura are supported by a fellowship for Japanese Junior Scientists from the Japan Society for the Promotion of Science.

Received for publication April 9, 2009, and accepted in revised form October 28, 2009.

Address correspondence to: Koji Eto, Division of Stem Cell Bank, The Institute of Medical Science, The University of Tokyo, 4-6-1 Shirokanedai, Minato-ku, Tokyo, 108-8639 Japan. Phone: 81-3-6409-2342; Fax: 81-3-6409-2343; E-mail: keto@ims.u-tokyo.ac.jp. Or to: Satoshi Takaki, Research Institute, International Medical Center of Japan, 1-21-1 Toyama, Shinjuku-ku, Tokyo, 162-8655 Japan. Phone: 81-3-3202-7181; Fax: 81-3-3208-5421; E-mail: stakaki@ri.imcj.go.jp.

1. Shattil SJ, Newman PJ. Integrins: dynamic scaffolds for adhesion and signaling in platelets. *Blood.* 2004;104(6):1606–1615.
2. Ruggeri ZM. Platelets in atherothrombosis. *Nat Med.* 2002;8(11):1227–1234.
3. Inoue O, et al. Laminin stimulates spreading of platelets through integrin alpha6beta1-dependent activation of GPVI. *Blood.* 2006;107(4):1405–1412.
4. Obergfell A, et al. Coordinate interactions of Csk, Src, and Syk kinases with [alpha]IIb[beta]3 initiate integrin signaling to the cytoskeleton. *J Cell Biol.* 2002;157(2):265–275.
5. Shattil SJ. Integrins and Src: dynamic duo of adhesion signaling. *Trends Cell Biol.* 2005;15(8):399–403.
6. Arias-Salgado EG, et al. PTP-1B is an essential positive regulator of platelet integrin signaling. *J Cell Biol.* 2005;170(5):837–845.
7. Prevost N, et al. Eph kinases and ephrins support thrombus growth and stability by regulating integrin outside-in signaling in platelets. *Proc Natl Acad Sci U S A.* 2005;102(28):9820–9825.
8. Law DA, et al. Integrin cytoplasmic tyrosine motif is required for outside-in alphaIIbbeta3 signalling and platelet function. *Nature.* 1999;401(6755):808–811.
9. Phillips DR, Nannizzi-Alaimo L, Prasad KS. Beta3 tyrosine phosphorylation in alphaIIbbeta3 (platelet membrane GP IIb-IIIa) outside-in integrin signaling. *Thromb Haemost.* 2001;86(1):246–258.
10. Xi X, et al. Tyrosine phosphorylation of the integrin beta 3 subunit regulates beta 3 cleavage by calpain. *J Biol Chem.* 2006;281(40):29426–29430.
11. Takaki S, et al. Control of B cell production by the adaptor protein lnk. Definition of a conserved family of signal-modulating proteins. *Immunity.* 2000;13(5):599–609.
12. Takaki S, Morita H, Tezuka Y, Takatsu K. Enhanced hematopoiesis by hematopoietic progenitor cells lacking intracellular adaptor protein, Lnk. *J Exp Med.* 2002;195(2):151–160.
13. Velazquez L, et al. Cytokine signaling and hematopoietic homeostasis are disrupted in Lnk-deficient mice. *J Exp Med.* 2002;195(12):1599–1611.
14. Tong W, Lodish HF. Lnk inhibits Tpo-mpl signaling and Tpo-mediated megakaryocytopoiesis. *J Exp Med.* 2004;200(5):569–580.
15. Tong W, Zhang J, Lodish HF. Lnk inhibits erythropoiesis and Epo-dependent JAK2 activation and downstream signaling pathways. *Blood.* 2005;105(12):4604–4612.
16. Buza-Vidas N, et al. Cytokines regulate postnatal hematopoietic stem cell expansion: opposing roles of thrombopoietin and LNK. *Genes Dev.* 2006;20(15):2018–2023.
17. Seita J, et al. Lnk negatively regulates self-renewal of hematopoietic stem cells by modifying thrombopoietin-mediated signal transduction. *Proc Natl Acad Sci U S A.* 2007;104(7):2349–2354.
18. Falati S, Gross P, Merrill-Skoloff G, Furie BC, Furie B. Real-time in vivo imaging of platelets, tissue factor and fibrin during arterial thrombus formation in the mouse. *Nat Med.* 2002;8(10):1175–1181.
19. Takizawa H, et al. Growth and maturation of megakaryocytes is regulated by Lnk/Sh2b3 adaptor protein through crosstalk between cytokine- and integrin-mediated signals. *Exp Hematol.* 2008;36(7):897–906.
20. Reddy KB, Smith DM, Plow EF. Analysis of Fyn function in hemostasis and alphaIIbbeta3-integrin signaling. *J Cell Sci.* 2008;121(Pt 10):1641–1648.
21. Fitau J, Boulday G, Coulon F, Quillard T, Charreau B. The adaptor molecule Lnk negatively regulates tumor necrosis factor-alpha–dependent VCAM-1 expression in endothelial cells through inhibition of the ERK1 and -2 pathways. *J Biol Chem.* 2006;281(29):20148–20159.
22. Ema H, et al. Quantification of self-renewal capacity in single hematopoietic stem cells from normal and Lnk-deficient mice. *Dev Cell.* 2005;8(6):907–914.
23. Dubois C, Panicot-Dubois L, Merrill-Skoloff G, Furie B, Furie BC. Glycoprotein VI-dependent and -independent pathways of thrombus formation in vivo. *Blood.* 2006;107(10):3902–3906.
24. Nishimura S, et al. In vivo imaging in mice reveals local cell dynamics and inflammation in obese adipose tissue. *J Clin Invest.* 2008;118(2):710–721.
25. Dubois C, Panicot-Dubois L, Gainor JF, Furie BC, Furie B. Thrombin-initiated platelet activation in vivo is vWF independent during thrombus formation in a laser injury model. *J Clin Invest.* 2007;117(4):953–960.
26. Furie B, Furie BC. In vivo thrombus formation. *J Thromb Haemost.* 2007;5(Suppl 1):12–17.
27. Juliano RL, Redding P, Alahari S, Edin M, Howe A, Aplin A. Integrin regulation of cell signaling and motility. *Biochem Soc Trans.* 2004;32(pt 3):443–446.
28. Blystone SD. Kinetic regulation of beta 3 integrin tyrosine phosphorylation. *J Biol Chem.* 2002;277(49):46886–46890.
29. Obergfell A, et al. The molecular adapter SLP-76 relays signals from platelet integrin alphaIIbbeta3 to the actin cytoskeleton. *J Biol Chem.* 2001;276(8):5916–5923.
30. Jordan MS, Singer AL, Koretzky GA. Adaptors as central mediators of signal transduction in immune cells. *Nat Immunol.* 2003;4(2):110–116.
31. Arias-Salgado EG, et al. Src kinase activation by direct interaction with the integrin beta cytoplasmic domain. *Proc Natl Acad Sci U S A.* 2003;100(23):13298–13302.
32. Salsmann A, Schaffner-Reckinger E, Kabile F, Plancon S, Kieffer N. A new functional role of the fibrinogen RGD motif as the molecular switch that selectively triggers integrin alphaIIbbeta3-dependent RhoA activation during cell spreading. *J Biol Chem.* 2005;280(39):33610–33619.
33. Petrich BG, et al. The antithrombotic potential of selective blockade of talin-dependent integrin alpha IIb beta 3 (platelet GPIIb-IIIa) activation. *J Clin Invest.* 2007;117(8):2250–2259.
34. Takizawa H, et al. Enhanced engraftment of hematopoietic stem/progenitor cells by the transient inhibition of an adaptor protein, Lnk. *Blood.* 2006;107(7):2968–2975.
35. Cancelas JA, et al. Rac GTPases differentially integrate signals regulating hematopoietic stem cell localization. *Nat Med.* 2005;11(8):886–891.
36. Weyrich AS, et al. Signal-dependent translation of a regulatory protein, Bcl-3, in activated human platelets. *Proc Natl Acad Sci U S A.* 1998;95(10):5556–5561.
37. Berrier AL, Martinez R, Bokoch GM, LaFlamme SE. The integrin beta tail is required and sufficient to regulate adhesion signaling to Rac1. *J Cell Sci.* 2002;115(Pt 22):4285–4291.
38. Arias-Salgado EG, Lizano S, Shattil SJ, Ginsberg MH. Specification of the direction of adhesive signaling by the integrin beta cytoplasmic domain. *J Biol Chem.* 2005;280(33):29699–29707.
39. Izuhara Y, et al. Inhibition of plasminogen activator inhibitor-1: its mechanism and effectiveness on coagulation and fibrosis. *Arterioscler Thromb Vasc Biol.* 2008;28(4):672–677.
40. Ono A, et al. Identification of a fibrin-independent platelet contractile mechanism regulating primary hemostasis and thrombus growth. *Blood.* 2008;112(1):90–99.
41. Brass LF, Zhu L, Stalker TJ. Novel therapeutic targets at the platelet vascular interface. *Arterioscler Thromb Vasc Biol.* 2008;28(3):s43–s50.
42. Hunt KA, et al. Newly identified genetic risk vari-

ants for celiac disease related to the immune response. *Nat Genet.* 2008;40(4):395–402.
43. Gudbjartsson DF, et al. Sequence variants affecting eosinophil numbers associate with asthma and myocardial infarction. *Nat Genet.* 2009;41(3):342–347.
44. Yagi T, et al. Regional localization of Fyn in adult brain; studies with mice in which fyn gene was replaced by lacZ. *Oncogene.* 1993;8(12):3343–3351.
45. Kasirer-Friede A, et al. ADAP is required for normal alphaIIbbeta3 activation by VWF/GP Ib-IX-V and other agonists. *Blood.* 2007;109(3):1018–1025.
46. Eto K, et al. The WAVE2/Abi1 complex differentially regulates megakaryocyte development and spreading: implications for platelet biogenesis and spreading machinery. *Blood.* 2007;110(10):3637–3647.
47. Prevost N, Kato H, Bodin L, Shattil SJ. Platelet integrin adhesive functions and signaling. *Methods Enzymol.* 2007;426:103–115.
48. Suzuki-Inoue K, et al. Involvement of Src kinases and PLCgamma2 in clot retraction. *Thromb Res.* 2007;120(2):251–258.

Published September 20, 2010

JEM

Article

Lnk-dependent axis of SCF–cKit signal for osteogenesis in bone fracture healing

Tomoyuki Matsumoto,[1,2] Masaaki Ii,[1,3] Hiromi Nishimura,[1] Taro Shoji,[1,2] Yutaka Mifune,[1,2] Atsuhiko Kawamoto,[1] Ryosuke Kuroda,[2] Tomoaki Fukui,[1,2] Yohei Kawakami,[1,2] Tomoya Kuroda,[1,2] Sang Mo Kwon,[1] Hiroto Iwasaki,[1] Miki Horii,[1] Ayumi Yokoyama,[1] Akira Oyamada,[1] Sang Yang Lee,[2] Shinya Hayashi,[2] Masahiro Kurosaka,[2] Satoshi Takaki,[4] and Takayuki Asahara[1,5]

[1]Group of Vascular Regeneration Research, Institute of Biomedical Research and Innovation, [2]Department of Orthopedic Surgery, Kobe University Graduate School of Medicine, [3]Department of Pharmacology, Osaka Medical College, 565-8686, Osaka, Japan

[4]Division of Immunology, Department of Microbiology and Immunology, Institute of Medical Science, University of Tokyo, Tokyo,113-0033, Japan

[5]Department of Regenerative Medicine Science, Tokai University School of Medicine, Kanagawa, 251-1193, Japan

The therapeutic potential of hematopoietic stem cells/endothelial progenitor cells (HSCs/EPCs) for fracture healing has been demonstrated with evidence for enhanced vasculogenesis/angiogenesis and osteogenesis at the site of fracture. The adaptor protein Lnk has recently been identified as an essential inhibitor of stem cell factor (SCF)–cKit signaling during stem cell self-renewal, and Lnk-deficient mice demonstrate enhanced hematopoietic reconstitution. In this study, we investigated whether the loss of Lnk signaling enhances the regenerative response during fracture healing. Radiological and histological examination showed accelerated fracture healing and remodeling in Lnk-deficient mice compared with wild-type mice. Molecular, physiological, and morphological approaches showed that vasculogenesis/angiogenesis and osteogenesis were promoted in Lnk-deficient mice by the mobilization and recruitment of HSCs/EPCs via activation of the SCF–cKit signaling pathway in the perifracture zone, which established a favorable environment for bone healing and remodeling. In addition, osteoblasts (OBs) from Lnk-deficient mice had a greater potential for terminal differentiation in response to SCF–cKit signaling in vitro. These findings suggest that inhibition of Lnk may have therapeutic potential by promoting an environment conducive to vasculogenesis/angiogenesis and osteogenesis and by facilitating OB terminal differentiation, leading to enhanced fracture healing.

CORRESPONDENCE
Takayuki Asahara:
asa777@is.icc.u-tokai.ac.jp

Abbreviations used: β-gal, β-galactosidase; AD, adipocyte; ALP, alkaline phosphatase; BMP, bone morphogenetic protein; BMT, BM transplantation; Cbfa1, core binding factor 1; CFU-O, CFU of OB; Col1A1, collagen1A1; EC, endothelial cell; EPC, endothelial progenitor cell; Erk, extracellular signal-related kinase; HSC, hematopoietic stem cell; KSL, cKit$^+$Sca1$^+$Lin$^-$; LDPI, laser Doppler perfusion imaging; micro-CT, micro-computed tomography; MNC, mononuclear cell; OB, osteoblast; OC, osteocalcin; PB, peripheral blood; SCF, stem cell factor; SDS, sodium dodecyl sulfate; SL, Sca1$^+$Lin$^-$; SSC, saline sodium citrate buffer; VCAM, vascular cell adhesion molecule; VE-cad, VE-cadherin.

Embryonic stem cells in the blastocyst stage have the potential to generate any terminally differentiated cells in the body; however, other adult stem cell types, including hematopoietic stem cells/progenitor cells (HSCs/HPCs), have limited potency for postnatal tissue/organ regeneration. The hematopoietic system has traditionally been considered unique among phenotypically characterized adult stem/progenitor cells (Slack, 2000; Blau et al., 2001; Korbling and Estrov, 2003) in that it is an organized, hierarchical system with multipotent, self-renewing stem cells at the top, lineage-committed progenitor cells in the middle, and lineage-restricted precursor cells, which give rise to terminally differentiated cells, at the bottom (Weissman, 2000). Recently, Takaki et al. (2002) reported that Lnk is expressed in hematopoietic cell lineages, and BM cells of Lnk-deficient mice are competitively superior in hematopoietic population to those of WT mice. They also clarified that not only HSC/HPC numbers but also the self-renewal capacity of some HSCs/HPCs were markedly increased in Lnk-deficient mice (Ema et al., 2005). In addition, they identified the functional domains of Lnk and developed a dominant-negative Lnk

The Rockefeller University Press $30.00
J. Exp. Med. Vol. 207 No. 10 2207-2223
www.jem.org/cgi/doi/10.1084/jem.20100321

The Journal of Experimental Medicine

Published September 20, 2010

mutant that inhibits the functions of Lnk that are endogenously expressed in the HSCs/HPCs and thereby potentiates the HPCs for engraftment (Takizawa et al., 2006). Lnk shares a pleckstrin homology domain, a Src homology 2 domain, and potential tyrosine phosphorylation sites with APS and SH-2B. It belongs to a family of adaptor proteins implicated in integration and regulation of multiple signaling events (Huang et al., 1995; Takaki et al., 1997; Yokouchi et al., 1997; Li et al., 2000; Ahmed and Pillay, 2003) and has also been suggested to act as a negative regulator in the stem cell factor (SCF)–c-Kit signaling pathway (Takaki et al., 2000, 2002).

In another category of regenerative medicine, bone formation and regeneration has been extensively researched to meet clinical demand. A biologically optimal process of fracture repair results in the restoration of normal structure and function in the injured skeletal tissue. Although most fractures heal within a certain time period with callus formation that bridges the fracture gap while bone repair takes place, a large number of patients with fractures lose valuable time because of disability or confinement, leading to a loss of productivity and income. Moreover, a significant amount (5–10%) of fractures fail to heal and result in delayed union or persistent nonunion (Marsh, 1998; Rodriguez-Merchan and Forriol, 2004). Among various causes of failed bone formation and remodeling, inappropriate neoangiogenesis is considered to be a crucial factor (Harper and Kalgsbrun, 1999; Colnot and Helms, 2001). Notably, appropriate vasculogenesis by BM endothelial progenitor cells (EPCs; Asahara et al., 1997) is emerging as a prerequisite for bone development and regeneration, and there appears to be a developmental reciprocity between endothelial cells (ECs) and osteoblasts (OBs; Karsenty and Wagner, 2002). We have recently proved a pathophysiological role and contribution of murine BM-derived $Sca1^+Lin^-$ (SL) cells, HSC/EPC-enriched fraction, for bone healing (Matsumoto et al., 2008). Another group has also reported the increase of $CD34^+/AC133^+$ cells in peripheral blood (PB) of patients with fracture, suggesting the contribution of PB EPCs to bone healing (Laing et al., 2007). However, previous studies have demonstrated that the majority of callus-formed cells in fracture were derived from the periosteum rather than from PB (Nakazawa et al., 2004), indicating a minor contribution of BM-derived cells to fracture healing. Moreover, periosteal cells, but not endosteal BM cells, have recently been shown to be competent to produce fracture callus (Colnot, 2009). Therefore, emerging the concept of enhanced osteogenesis/angiogenesis by HSCs/EPCs, one of the novel factors responsible for stem/progenitor cell mobilization from BM, that is Lnk, attracted our research interests to develop therapeutic strategy using circulating EPCs for bone fracture.

SCF has already been reported to stimulate proliferation and differentiation of HSCs (Broudy, 1997) and mobilize HSCs/EPCs into PB (Mauch et al., 1995; Takahashi et al., 1999) by binding with cKit. Thus, we have investigated the hypothesis that a lack of Lnk signaling, dependent on the SCF–cKit signaling pathway, enhanced the regenerative response via vasculogenesis and osteogenesis in fracture healing by HSC/EPC mobilization and recruitment to sites of fracture in Lnk-deficient mice. In our series of experiments, we showed that a negatively controlled Lnk system contributed to a favorable environment for fracture healing by enhancing vasculogenesis/angiogenesis and osteogenesis via activation of SCF–cKit signaling pathway, which leads to prompt recovery from fracture. In contrast, cKit expression was observed in several tissues and cells, including OBs (Bilbe et al., 1996).

This is the first study showing interaction between the Lnk system and fracture healing that provides a new insight into negatively controlling the Lnk system not only to promote an environment conducive to vasculogenesis/angiogenesis and osteogenesis but also to up-regulate the potential of OB terminal differentiation so that fractures can promptly heal. Therefore, negatively regulating the Lnk system has important implications for the formulation of new therapeutic strategies to enhance bone repair.

RESULTS

Pre- and post-fracture phenotypic characterization of BM and PB

We first attempted to compare the frequency of BM HSC/EPC fraction identified as $cKit^+SL$ (KSL) cells at pre-fracture and 7 d after fracture in Lnk KO mice and age-matched WT mice (C57BL/6). The percentage of BM KSL fraction was significantly higher in post-fracture bone than in pre-fracture bone, regardless of mouse phenotype; however, it was significantly high in both pre- and post-fracture bone in Lnk KO mice compared with WT mice (pre-fracture: Lnk KO, 19.3 ± 0.5, WT, 5.6 ± 0.2; post-fracture: Lnk KO, 23.7 ± 0.5, WT, 8.3 ± 0.4%, respectively; $P < 0.05$ for Lnk KO vs. WT in both pre- and post-fracture bone; pre- vs. post-fracture bone in both Lnk KO and WT; $n = 5$; Fig. 1 a). Also, the number of KSL cells in 10^5 of PB mononuclear cells (MNCs) was significantly greater in post-fracture bone than in pre-fracture bone, regardless of mouse phenotype, and it was significantly great in both pre- and post-fracture PB in Lnk KO mice compared with WT mice (prefracture: Lnk KO, 1,141.4 ± 192.0; WT, 581.9 ± 97.7, post-fracture: Lnk KO, 1,467.1 ± 235.2; WT, 941.9 ± 300.0, respectively; $P < 0.01$ for Lnk KO vs. WT in both pre- and post-fracture; $P < 0.05$ for pre- vs. post-fracture in both Lnk KO and WT; $n = 5$; Fig. 1 b).

We next investigated which cell populations were mobilized into PB under fracture stress. Because the KSL cell population is extremely small in PB, there was no significant difference between the number and the percentage in PB at prefracture and 7 d post-fracture (unpublished data). We therefore attempted to make a comparison of the frequency of PB HSC/EPC-enriched fraction identified as cells at prefracture, 1, 4, 7, and 14 d after fracture in Lnk KO and WT mice. The percentage of post-fracture HSC/EPC-enriched fraction in PB was significantly higher, peaking at day 1 in both Lnk KO and WT mice, than that of pre-fracture (pre-fracture: Lnk KO, 39.7 ± 3.1, WT, 44.9 ± 0.8; 1 d post-fracture: Lnk KO, 56.2 ± 1.6, WT, 59.3 ± 3.1; 4 d post-fracture: Lnk KO, 53.5 ± 3.0, WT, 57.7 ± 1.1; 7 d post-fracture: Lnk KO, 43.8 ± 4.1, WT,

Published September 20, 2010

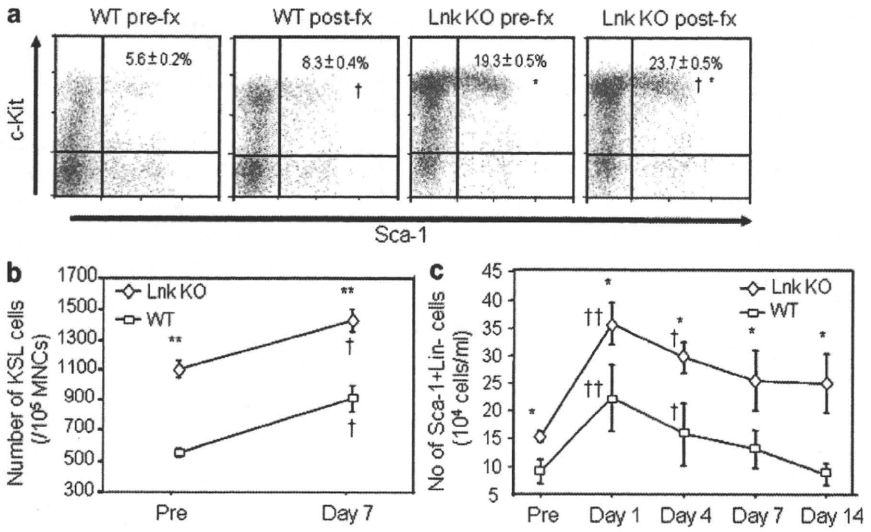

Figure 1. Phenotypic characterization of BM and PB pre- and post-fracture. (a) The percentage of KSL fraction in BMMNCs was assessed by FACS analysis at pre- and 7 d post-fracture (fx) stage in WT and Lnk KO mice, and expressed on the top right quadrant of the dot-blot graph. *, $P < 0.05$ versus WT; †, $P < 0.05$ vs. pre-fx. (b) The number of KSL cells in BMMNCs was also assessed by FACS at pre- and 7 d post-fx stage in WT (open square) and Lnk KO (open rhombus) mice. **, $P < 0.01$ vs. WT; †, $P < 0.05$ vs. pre-fx. (c) The number of SL cells in 1 ml of PB was assessed by FACS in WT (open square) and Lnk KO (open rhombus) mice in the indicated time course. ††, $P < 0.01$; †, $P < 0.05$ versus pre-fx; *, $P < 0.05$ versus WT. All data averaged from five independent experiments. All the mean values with SEM were obtained from triplicated assays.

55.0 ± 1.2; 14 d post-fracture: Lnk KO, 41.0 ± 1.9, WT, 52.6 ± 2.4%; $P < 0.01$ for pre-fracture vs. 1 d post-fracture in both Lnk KO and WT; $P < 0.05$ for pre-fracture vs. 4 d post-fracture in both Lnk KO and WT; $n = 5$). The number of post-fracture SL cells per 1 ml of PB was significantly high, peaking at day 1 compared with pre-fracture (pre-fracture: Lnk KO, 15.1 ± 1.0, WT, 7.2 ± 1.1; 1 d post-fracture: Lnk KO, 35.6 ± 3.7, WT, 22.1 ± 6.1; 4 d post-fracture: Lnk KO, 29.5 ± 2.8, WT, 15.6 ± 9.7; 7 d post-fracture: Lnk KO, 25.3 ± 5.4, WT, 13.7 ± 1.9; 14 d post-fracture: Lnk KO, 24.8 ± 5.4, WT, 8.4 ± 1.9 × 10^4 cells/ml; $P < 0.01$ for pre-fracture vs. 1 d post-fracture in both Lnk KO and WT; $P < 0.05$ for pre-fracture vs. 4 d post-fracture in both Lnk KO and WT, Lnk KO vs. WT at each time point; $n = 5$; Fig. 1 c). These results indicate that both fracture stress and lack of Lnk induce the mobilization of SL cells, including KSL cells from BM, resulting in a high SL/KSL cell number in PB in Lnk KO fractured mice compared with that in WT mice.

Tie2⁺ stem/progenitor cell contribution to vasculogenesis and osteogenesis

Based on the aforementioned evidence, we looked for BM-derived Tie2⁺ stem/progenitor cells in sites of fracture using a mouse BM transplantation (BMT) model. First, we generated Tie2/LacZ Lnk KO mice, in which the LacZ gene is expressed under the regulation of promotor Tie2 (lacking the Lnk gene), by crossing Tie2/LacZ transgenic and Lnk KO mice. We then performed BMT from Tie2/LacZ Lnk KO mice to Lnk KO mice and from Tie2/LacZ WT mice to WT mice. Fracture was induced 4 wk after BMT, after reconstitution of BM with Tie2/LacZ Lnk KO cells in Lnk KO and WT mice, and granulation tissue was analyzed histologically in sites of fracture 7 d after surgery. Double-fluorescent immunostaining was performed for β-galactosidase (β-gal), which can detect BM-derived Tie2⁺ cells and CD31, an EC marker, or for β-gal and osteocalcin (OC). The β-gal⁺ and CD31 double-positive ECs were frequently observed in Tie2/LacZ Lnk KO-BMT Lnk KO mice, whereas the double-positive cells were rarely identified in Tie2/LacZ WT-BMT WT mice (Fig. 2 a). The number of double-positive cells was significantly increased in Tie2/LacZ Lnk KO-BMT Lnk KO mice compared with that in Tie2/LacZ WT-BMT WT mice (Lnk KO, 410.0 ± 37.6 vs. WT, 230.0 ± 56.7/mm²; $P < 0.05$; $n = 3$; Fig. 2 b). The β-gal⁺ and OC double-positive OBs were frequently observed as lining cells along with newly formed bone surface in Tie2/LacZ Lnk KO-BMT Lnk KO mice, whereas only a few double-positive cells were identified in Tie2/LacZ WT-BMT WT mice. (Fig. 2 a) The number of double-positive cells was significantly increased in Tie2/LacZ Lnk KO-BMT Lnk KO mice compared with that in Tie2/LacZ WT-BMT WT mice (Lnk KO, 195.0 ± 31.0 vs.WT, 105.0 ± 21.5/mm²; $P < 0.05$; $n = 3$; Fig. 2 c). These results suggest that enhanced recruitment of mobilized Tie2⁺ stem/progenitor cells to fracture sites contributes to vasculogenesis and osteogenesis, leading to accelerated fracture healing in Lnk KO mice.

BM-derived SL cells exhibit multilineage differentiation potential in vitro

To explore whether SL cells have multilineage differentiation potential, specifically to ECs, OBs, and adipocytes (ADs), BM-derived SL cells were cultured in differentiation induction medium for each lineage, and each marker expression was examined by real-time RT-PCR and immunocytochemistry after culture for 7 and 14 d, respectively. The mRNA expression of EC markers (CD31: 243.8 ± 7.3 vs. 372.1 ± 7.0, $P < 0.05$, $n = 3$; vWF: 49.1 ± 1.0 vs. 396.0 ± 24.1, $P < 0.01$, $n = 3$; Fig. 2 d), OB markers (OC: 6.7 ± 0.8 vs. 182.6 ± 9.5, $P < 0.001$, $n = 3$; Collagen 1-A1: 784.6 ± 107.8 vs. 22,667 ± 2,114, $P < 0.001$, $n = 3$; Fig. 2 e), and AD markers (LPL: 1.4 ± 0.1 vs. 642.0 ± 17.2, $P < 0.0001$, $n = 3$; PPARγ: 7.1 ± 0.3 vs. 162.7 ± 6.7, $P < 0.0001$, $n = 3$; Fig. 2 f) were significantly up-regulated by culture with each lineage induction medium. These lineage marker expressions were further confirmed by

Published September 20, 2010

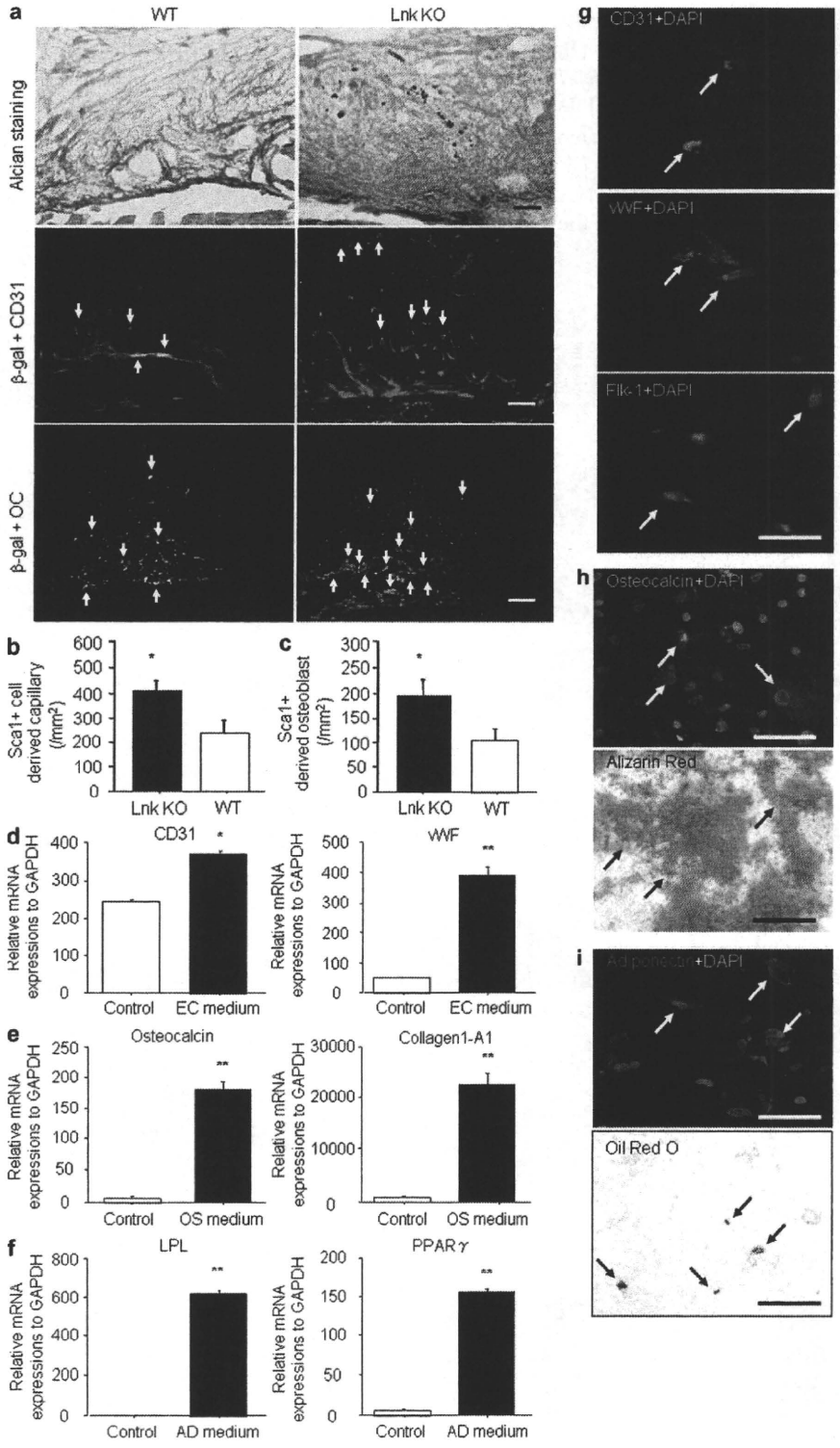

Figure 2. Immunohistochemical detection of Tie2/β-gal⁺ BM-derived stem/progenitor cells in sites of fracture and multilineage differentiation capacity of SL BM cells. (a) Double-immunofluorescent staining for β-gal (red) and CD31 (green) and β-gal (red) and OC (OC, green) were performed in peri-fracture sites 7 d after surgery in Lnk KO mice (left) and WT mice (right). Arrows indicate β-gal/CD31 and β-gal/OC double-positive capillaries and OBs, respectively. Alcian blue/orange G–stained sections were also shown in parallel with immunostained sections. (a, top) Dotted line indicates bone surface. Bars, 50 µm. Quantification of β-gal⁺ ECs (b) and OBs (c). β-gal and CD31 or OC double-positive cells were counted in three randomly selected high-power fields and averaged. *, $P < 0.05$ versus WT. EC (d; CD31 and vWF), OB (e; OC and collagen 1-A1), and AD (f; LPL and PPARγ) marker gene expressions were assessed by real-time RT-PCR in SL cells cultured for 7 d with each cell lineage differentiation medium (*, $P < 0.05$; **, $P < 0.001$) and fluorescent immunostaining analyses with CD31 and vWF for ECs (g), OC for OBs for OBs (h), and LPL and PPARγ for ADs (i) were also performed in SL cells after 14 d in culture. The differentiated SL cells were also stained with alizarin red (h) and oil red O (i) for detecting OB and AD, respectively. Bars, 50 µm. Arrows indicate staining of positive cells. All data averaged with SEM from three independent experiments. All experiments were obtained from triplicated assays.

immunopositivities for CD31, vWF, Flk-1 (Fig. 2 g), OC (Fig. 2 h), and adiponectin (Fig. 2 i) in SL cells. The alizarin red and oil red O staining also show characteristics of OBs and ADs, respectively (Fig. 2, h and i).

Molecular evidence of enhanced angiogenesis and osteogenesis in Lnk KO mice

To explore specific gene expression differences under fracture stress between Lnk-deficient and WT mice, angiogenesis (96)– and osteogenesis (96)–related genes of the tissue at the fracture site spotted on cDNA microarrays were hybridized with biotin-labeled cDNA probes according to the manufacturer's instructions. In angiogenesis gene array, relative expression levels of 12 genes (*ANG*, *Fisp12* [*Ctgf*], *VEGFR*[*Flt1*], *HGF*, *IL-10*, *Gelatinase B* [*Mmp9*], *SR-A* [*Msr1*], *Restin* [*Rsn*], *BM40* [*Sparc*], *ALK-5* [*Tgfbr1*], *THBS1*, and *VCAM-1*) of Lnk-deficient fractured mice increased by >1.5-fold, but 5 genes (*Ephrin B4* [*Ephb4*], *IFNr* [*Ifng*], *NOS3*, *Osteopontin* [*Spp1*], and *THBS2*) decreased by >2-fold compared with WT fractured mice (Fig. 3 a). In osteogenesis gene array, 24 genes (*annexin A5* [*Anxa5*], *OC* [*Bglap1*], *Bgn*,

Published September 20, 2010

Alk-6 [*Bmpr1a*], *BMPR2*, *Col11a1*, *Col1a1*, *Col1A2*, *Col4a6*, *Col6a2*, *Ctsk*, *Dcn*, *FLG* [*Fgfr1*], *Smad2* [*Madh1*], *Smad3* [*Madh3*], *Collagenase-3* [*Mmp13*], *MMP8*, *Gelatinase B* [*Mmp9*], *Osf2/Cbfa1* [*Runx2*], *SPARC*, *TGFb3*, *ALK-5* [*Tgfbr1*], *VCAM-1*, and *Vdr*) of Lnk-deficient fractured mice increased by >1.5-fold compared with WT fractured mice ($n = 3$; Fig. 3 b).

Real time RT-PCR analysis of the tissue that was RNA isolated from the peri-fracture site was also performed in the expression of several key genes as a quantitative analysis. The results demonstrated a significantly higher expression of EC markers (CD31, VE-cadherin [VE-cad], and KDR/Flk1) in Lnk KO group compared with WT group (CD31: Lnk KO, 5.803 ± 0.667, WT, 1.171 ± 0.029, $P < 0.01$; VE-cad: Lnk KO, 7.693 ± 0.602, WT, 1.244 ± 0.006, $P < 0.01$; KDR: Lnk KO, 11.082 ± 1.036, WT, 1.415 ± 0.035, respectively, $P < 0.01$; $n = 3$; Fig. 3 c). The expression of bone-related

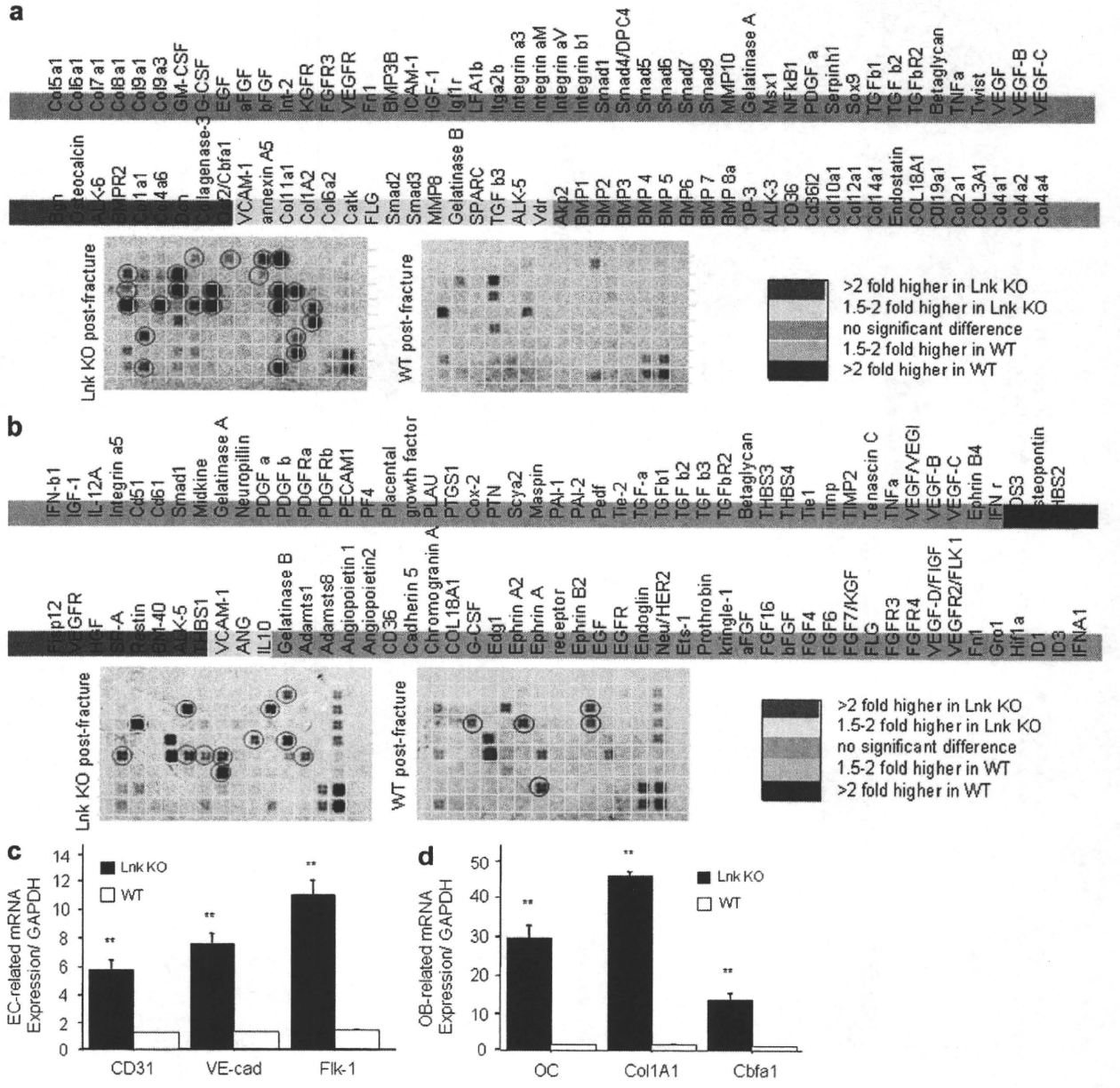

Figure 3. Angiogenesis- and osteogenesis-related gene expressions in sites of fracture. (a and b) A series of gene expressions detected by DNA microarray analysis in granulation tissue samples of peri-fracture sites 7 d after surgery in Lnk KO and WT mice. Red circles indicate >1.5-fold and blue circles do over 2-fold-increased blots in Lnk KO mice compared with WT mice. The selected EC-related (c) and OB-related (d) gene up-regulation in the same samples as those in DNA microarray analysis were further confirmed by quantitative real-time RT-PCR analysis. VE-cad, Flk-1 (VEGF receptor 2); Col1A1, Col1A1; and Cbfa1, Cbfa1. **, $P < 0.01$ versus WT. All data averaged with SEM from three independent experiments. All experiments were obtained from triplicated assays.

Published September 20, 2010

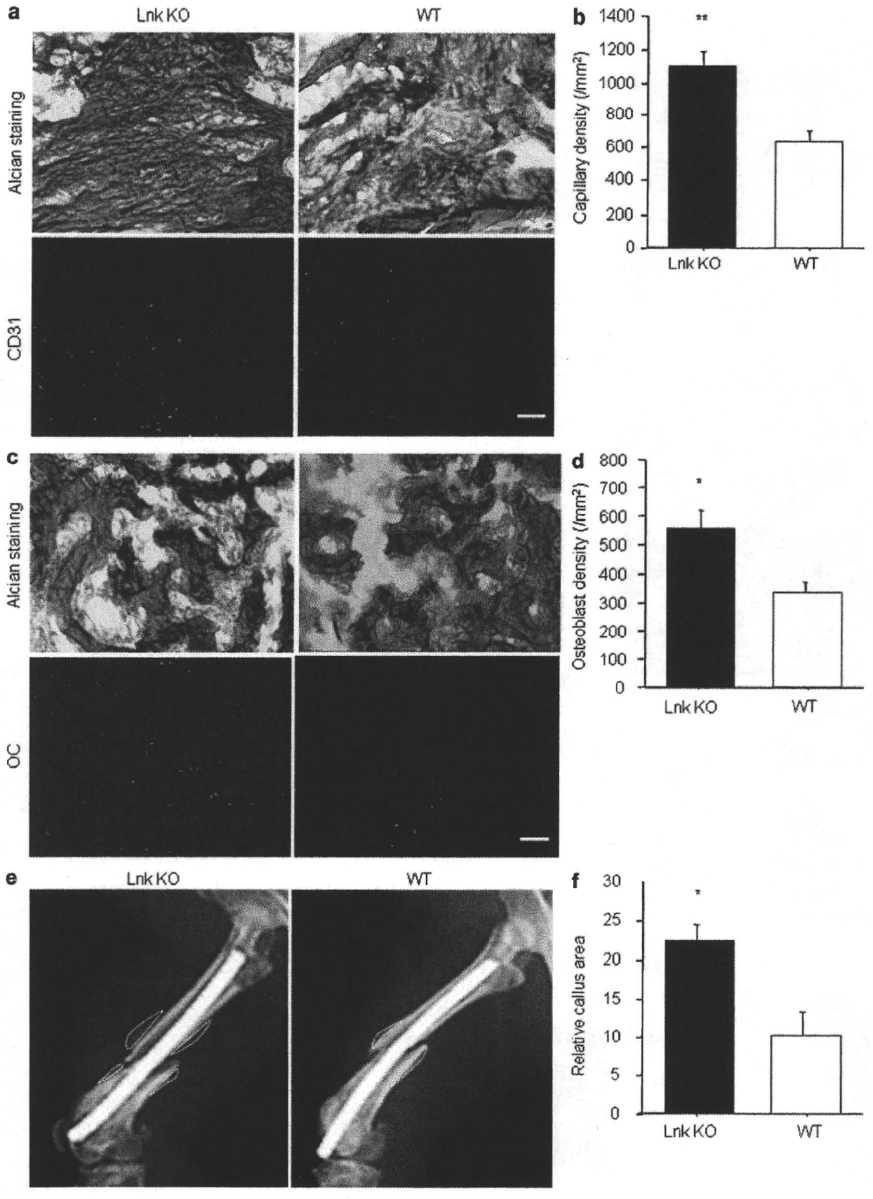

Figure 4. Histological and radiographical evidences of enhanced angiogenesis/vasculogenesis and osteogenesis in Lnk KO fractured mice. Immunofluorescent staining for CD31 (green; a) and OC (OC, green; c) were performed in granulation tissue samples of peri-fracture sites in Lnk KO (left) and WT (right) mice 7 d after fracture. Alcian blue/orange G-stained sections were also shown in parallel with immunostained sections. (bottom) Dotted line indicates bone surface. Bar, 50 µm. Quantification of capillaries (b) and OBs (d). CD31 positive capillaries and OC positive OBs were counted in 3 randomly selected high power fields and averaged. **, $P < 0.01$ versus WT. (e) Radiographical assessment of callus area in sites of fracture 7 d after surgery. Callus area is indicated in dotted line. (f) Relative callus areas are quantified and averaged. *, $P < 0.05$ versus WT. All data averaged with SEM from three independent experiments. All experiments were obtained from triplicated assays.

markers (OC, collagen1A1 [Col1A1], and Core binding factor 1 [Cbfa1]) were significantly enhanced in Lnk KO group compared with WT group (OC: Lnk KO, 29.707 ± 3.116, WT, 1.294 ± 0.056, $P < 0.01$; Col1A1: Lnk KO, 46.189 ± 0.870, WT, 1.225 ± 0.225, $P < 0.01$; Cbfa1: Lnk KO, 13.586 ± 1.767; WT, 0.999 ± 0.049, $P < 0.01$; $n = 3$; Fig. 3 d). These results indicate the enhancement of osteogenesis, as well as angiogenesis, at fracture sites in Lnk KO mice.

Morphological evidence of enhanced angiogenesis and osteogenesis in fractured Lnk KO mice

Enhanced angiogenesis and osteogenesis were further confirmed by immunohistochemistry. Vascular staining with CD31 (marker for mouse EC) 7 d after fracture demonstrated enhanced neovascularization around the endochondral ossification area in Lnk KO mice compared with that in WT mice (Fig. 4 a). Neovascularization assessed by capillary density was significantly enhanced in Lnk KO mice compared with that in WT mice (Lnk KO, 1,101.8 ± 97.7 vs. WT, 628.7 ± 28.5/mm²; $P < 0.01$; $n = 3$; Fig. 4 b).

OB staining with OC (marker for mouse OB) 7 d after fracture also revealed the augmentation of osteogenesis in newly formed bone area in Lnk KO mice compared with WT mice (Fig. 4 c). Osteogenesis assessed by OB density was significantly enhanced in Lnk KO mice compared with WT mice (Lnk KO, 111.7 ± 13.2, WT, 66.7 ± 6.5/mm²; $P < 0.05$; $n = 3$; Fig. 4 d). Callus formation was monitored radiographically to evaluate fracture healing process, and the relative callus areas detected by radiography were quantified at week 1 in Lnk KO and WT group (Fig. 4 e). The relative callus area was significant larger in the Lnk KO group compared with the WT group (Lnk KO, 22.3 ± 2.0, WT, 10.0 ± 3.0; $P < 0.05$; $n = 3$; Fig. 4 f). These results indicate the morphological enhancement of angiogenesis and osteogenesis in Lnk KO mice compared with WT mice in fracture-induced environment.

Physiological, radiological, and histological evidences of promoted fracture healing in Lnk KO mice

Blood perfusion and morphological fracture healing in each group was evaluated by laser Doppler perfusion imaging (LDPI)

Published September 20, 2010

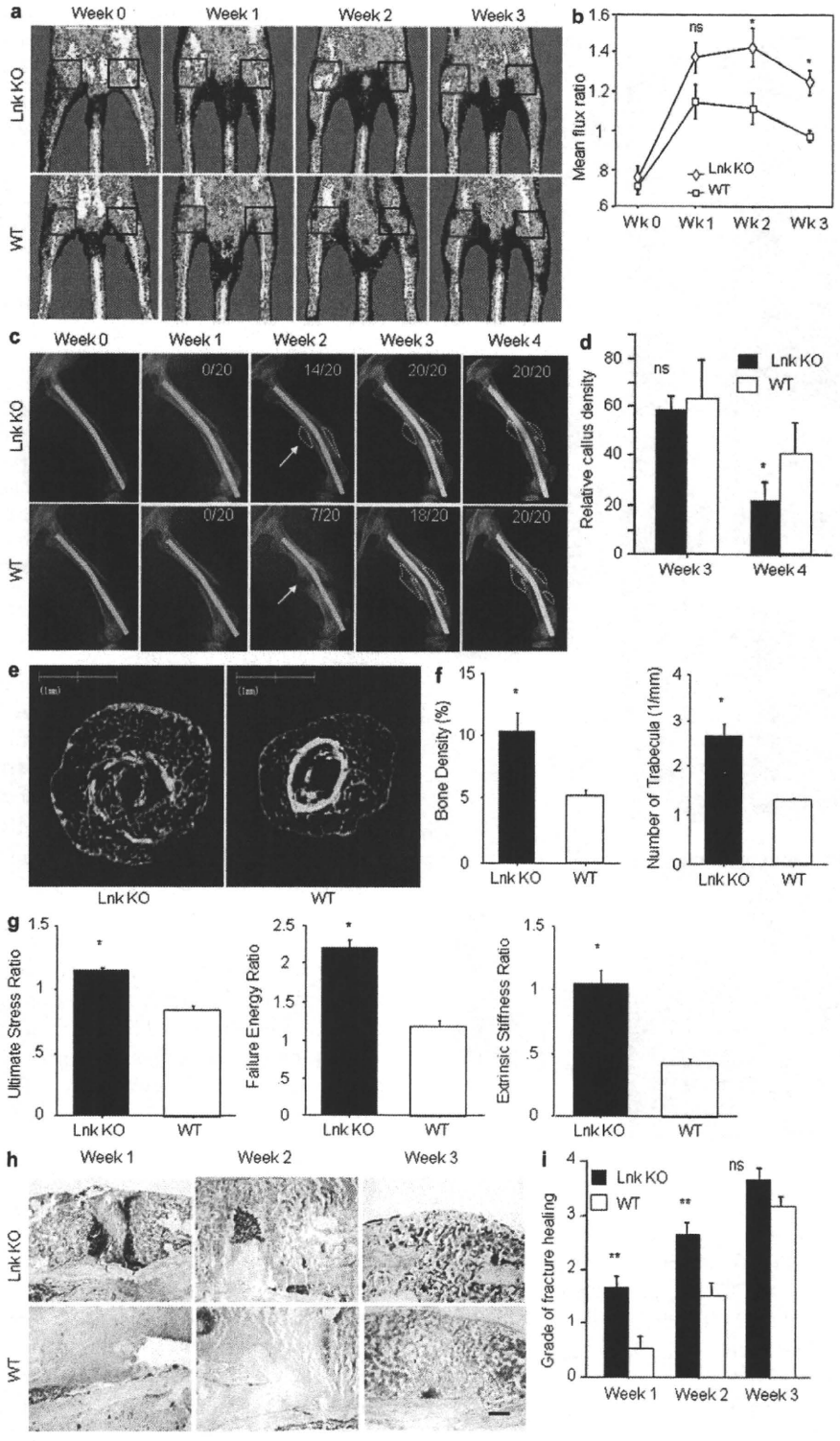

Figure 5. Increased blood perfusion and radiographically accelerated fracture healing in Lnk KO mice. (a) Tissue blood perfusion evaluated by LDPI system after surgery in the indicated time course. The fractured sites are indicated in red square and intact contra-lateral sites are indicated in black square. (b) The mean flux-ratio was calculated by dividing mean flux value in red square with that in blue square and expressed as a relative mean flux value. **, $P < 0.01$ versus Week 0 and *, $P < 0.05$ versus WT. Data averaged with SEM from four independent experiments. Radiographical (c and e) and histological (f) assessment during fracture healing process in Lnk KO (left) and WT (right) mice. (c) Callus area is indicated in dotted line and the number of healed bones out of 20 is indicated in upper right corner of the image. Arrows indicate fracture sites. (d) The number of relative callus density is quantified. * and ns, $P < 0.05$ versus WT, $n = 20$ each. (e) The bone structure after healing was further assessed by micro CT 28 d after surgery. (f) Bone density and number of trabecular bones were quantified in the micro CT images and averaged. *, $P < 0.05$ versus WT. Data averaged with SEM from four independent experiments. (g) Biomechanical function test for healed bone in Lnk KO and WT mice 28 d after fracture. Each parameter, ultimate stress (left), fracture energy (center) and extrinsic stiffness ratio (right), was evaluated as healed bone function. *, $P < 0.05$ versus WT. Data averaged with SEM from four independent experiments. (h) Toluidine blue staining was performed with granulation tissue at fracture site in the indicated time course. Chondrocytes are stained in blue and bone including newly formed trabecular bone is appeared in gray. Bar = 200 µm. (i) The degree of fracture healing in the toluidine blue stained sections was assessed by Allen's classification in Lnk KO and WT mice. ** and ns, $P < 0.01$ versus WT. Data averaged with SEM from six independent experiments.

system and radiological examinations at subsequent time points after fracture. LDPI analysis (Fig. 5 a) demonstrated a severe loss of blood flow at the fracture sites 1 h after fracture creation in both groups. However, the blood flow of the fractured limb increased until 2 wk post-fracture, and then decreased slowly in KO mice. In WT mice, the blood flow showed a mild increase until 1 wk post-fracture, and then decreased. In both groups, the ratio of fractured/intact (contralateral) blood flow significantly increased by week 1 (Fig. 5 b). There was no significant difference in the ratio 1 h after fracture creation between the groups, whereas the ratio at weeks 1, 2, and 3 were significantly higher in Lnk KO mice compared with WT mice (0 wk: Lnk KO, 0.753 ± 0.067, WT,

0.707 ± 0.045; 1 wk: Lnk KO, 1.370 ± 0.081, WT, 1.144 ± 0.088; 2 wk: Lnk KO, 1.425 ± 0.103, WT, 1.110 ± 0.077; 3 wk: Lnk KO, 1.241 ± 0.064, WT, 0.972 ± 0.030; $P < 0.01$ for week 0 vs. weeks 1–3 in both Lnk KO and WT; $P < 0.05$ for Lnk KO vs. WT in week 1–3; $n = 4$ mice/group/time-point; Fig. 5 b).

In 70% (14 out of 20) of Lnk KO mice at week 2 and 100% (20 out of 20) at week 3, the fracture healed with bridging callus formation radiographically, whereas in WT mice only 35% (7 out of 20) had healed at week 2 and 90% (18 out of 20) at week 3 ($P < 0.05$ in week 2; Fig. 5 c), which is consistent with the data in previous studies demonstrating the natural course in this animal model (Manigrasso and O'Connor, 2004). To evaluate bone remodeling, bone absorption was monitored radiographically and relative callus density was quantified at week 3 and 4 in Lnk KO and WT group. Relative callus density was significantly lower in Lnk KO group compared with that in WT group (3 wk: Lnk KO, 58.1 ± 2.4 vs. WT, 62.2 ± 6.8, ns; 4 wk: Lnk KO, 22.5 ± 2.8 vs. WT, 40.2 ± 5.3, $P < 0.05$, $n = 20$; Fig. 5 d).

Morphological and functional fracture healing in each group was further evaluated by micro-computed tomography (micro-CT), histological analysis, and biomechanical examination 28 d after fracture surgery. The micro-CT results showed striking trabecular bone formation in Lnk KO mice compared to that in WT mice (Fig. 5 e). Quantitative analysis for bone formation was performed with micro-CT images and expressed as bone density (Fig. 5 f, left) and trabecula number (Fig. 5 f, right). Both parameters were significantly high in Lnk KO mice compared with that in WT mice (bone density: Lnk KO, 10.4 ± 1.5 vs. WT, 5.0 ± 0.3, $P < 0.05$, $n = 4$; number of trabecular: Lnk KO, 2.7 ± 0.3 vs. WT, 1.3 ± 0.03, $P < 0.01$, $n = 4$; Fig. 5 f). Biomechanical examinations by three-point bending test also showed significantly increased ultimate stress ratio (Lnk KO, 1.2 ± 0.02 vs. WT, 0.8 ± 0.03, $P < 0.001$, $n = 4$), failure energy ratio (Lnk KO, 2.2 ± 0.1 vs. WT, 1.2 ± 0.1, $P < 0.001$, $n = 4$), and extrinsic stiffness ratio (Lnk KO, 1.1 ± 0.1 vs. 0.4 ± 0.04, $P < 0.01$, $n = 4$; Fig. 5 g).

Histological evaluation with toluidine blue staining demonstrated the enhanced endochondral ossification consisting of numerous chondrocytes and newly formed trabecular bone at week 1, bridging callus formation at week 2, and complete union at week 3 in Lnk KO mice. In contrast, although a callus formation was observed at week 1, bridging callus formation was rarely found at week 2 in WT mice (Fig. 5 h). The degree of fracture healing assessed by Allen's classification (Allen et al., 1980) was significantly higher in the Lnk KO group compared with the WT group at week 1 and 2 (1 wk: Lnk KO, 1.67 ± 0.21 vs. WT, 0.50 ± 0.22; 2 wk: Lnk KO, 2.67 ± 0.21 vs. WT, 1.50 ± 0.22, $P < 0.01$, $n = 6$; 3 wk: Lnk KO, 3.67 ± 0.21 vs. WT, 3.17 ± 0.17, ns, $n = 6$; Fig. 5 i). These results indicate that Lnk KO mice have a potential for prompt fracture healing evaluated by not only radiographical analysis but also biomechanical functional examination.

Critical role of SCF–cKit signaling in enhanced SL cell mobilization from BM and recruitment to sites of fracture

Although the aforementioned results clearly demonstrated enhanced vasculogenesis/angiogenesis and osteogenesis via SL or $Tie2^+$ cell mobilization into PB and recruitment to sites of fracture in Lnk KO mice, the precise mechanism remains unclear. To explore the possible mechanism, we focused on the role of the stem/progenitor cell chemokine SCF, which is a ligand for the receptor cKit, in Lnk KO mice as well as in WT mice. Accordingly, mouse (m) SCF plasma levels were measured before and after fracture at subsequent time points in both types of mice. The plasma SCF levels were decreased after fracture surgery regardless of Lnk gene deficiency in mice; however, the extent of decrease was significantly limited during the fracture healing process and returned to over the baseline level at day 14 in Lnk KO mice compared with that in WT mice (prefracture: Lnk KO, 263.4 ± 9.4 vs. WT, 251.0 ± 35.6 pg/ml; ns and 1 d post-fracture: Lnk KO, 194.1 ± 11.7 vs. WT, 166.8 ± 12.7 pg/ml; 4 d post-fracture: Lnk KO, 197.7 ± 7.2 vs. WT, 181.5 ± 28.9 pg/ml; 7 d post-fracture: Lnk KO, 214.7 ± 20.6 vs. WT, 190.7 ± 24.0 pg/ml; and 14 d post-fracture: Lnk KO, 284.2 ± 19.7 vs. WT, 207.3 ± 16.6 pg/ml; $P < 0.01$ for each comparison; $n = 5$; Fig. 6 a).

Next, the gain and loss of function test of SCF for SL cell mobilization in PB was performed by FACS analysis. We intraperitoneally injected 20 μg/kg mSCF, soluble SCF receptor (sKit, antagonist of SCF; Turner et al., 1995; Nakamura et al., 2004), or PBS into unfractured Lnk KO or WT mice for 5 d and examined SL cell kinetics in PB. The number of SL cells significantly increased, peaking at day 7 after SCF stimulation in Lnk KO mice, but not in WT mice, and no SL cell number increase was observed in the other treatment groups (sKit treatment in Lnk KO mice and PBS treatment in Lnk KO mice and in WT mice; prestimulation: Lnk KO-PBS, 13.0 ± 1.3; Lnk KO-SCF, 13.1 ± 0.7; Lnk KO-sKit, 15.3 ± 0.2; WT-PBS, 8.1 ± 0.9; WT-SCF, 8.7 ± 0.6 × 10^4 cells/ml, ns, $n = 5$; 7 d post-stimulation: Lnk KO-SCF, 73.4 ± 4.1 vs. Lnk KO-PBS, 15.3 ± 2.5; Lnk KO-sKit, 10.0 ± 0.8; WT-PBS, 8.3 ± 0.3; and WT-SCF, 12.8 ± 2.4 × 10^4 cells/ml, $P < 0.05$, $n = 5$; and 14 d post-fracture: Lnk KO-SCF, 39.2 ± 6.2 vs. Lnk KO-PBS, 13.6 ± 9.7; Lnk KO-sKit, 12.0 ± 0.3; WT-PBS, 7.9 ± 0.9; and WT-SCF, 10.0 ± 0.9 × 10^4 cells/ml, $P < 0.01$, $n = 5$; Fig. 6 b). Next, to identify the synergistic effect of fracture stress and SCF stimulation on SL cell mobilization, SCF with or without sKit and PBS was injected into fractured WT mice, and sKit alone was injected into fractured Lnk KO mice in the same way. In the fractured WT mice, the number of SL cells was significantly increased, peaking at day 7 post-stimulation by SCF, but not by PBS, whereas no response of SL cell number was observed in nonfractured WT mice by SCF, and the effect of SCF on SL cell mobilization was completely cancelled by coinjection of sKit. The inhibitory effect of sKit on SL cell mobilization in PB was also observed partially in Lnk KO mice with fracture (prestimulation: Lnk KO-sKit-Fx, 16.7 ± 2.1 vs. WT-PBS-Fx, 9.0 ± 2.1; WT-SCF-Fx, 8.3 ± 0.7; and WT-SCF-sKit-Fx, 9.8 ± 0.7 × 10^4 cells/ml, $P < 0.05$,

Published September 20, 2010

$n = 5$; 7 d post-stimulation: WT-SCF-Fx, 34.1 ± 1.4 vs. WT-PBS-Fx, 12.9 ± 3.3 and WT-SCF-sKit-Fx, 8.0 ± 1.0 × 10^4 cells/ml, $P < 0.01$, $n = 5$, [Lnk KO-sKit-Fx, 22.1 ± 3.4 × 10^4]; 14 d post-fracture: WT-SCF-Fx, 17.9 ± 2.0 vs. WT-PBS-Fx, 8.5 ± 1.9 and WT-SCF-sKit-Fx, 7.7 ± 1.3 × 10^4 cells/ml, $P < 0.05$, $n = 5$, [Lnk KO-sKit-Fx, 15.0 ± 4.8 × 10^4]; Fig.6 c).

We further confirmed that SCF-induced stem/progenitor cell mobilization mediated enhanced angiogenesis and osteogenesis in sites of fracture by SCF–cKit signaling inhibition study in vivo. The mSCF (20 μg/kg/day), sKit (20 μg/kg/day), or PBS was injected intraperitoneally into mice with fracture for 5 d, and angiogenesis/osteogenesis was evaluated by immunofluorescent staining for CD31 and OC 7 d after surgery (Fig. 6 d). As we expected, SCF stimulation significantly increased both $CD31^+$ capillary density ($WT\text{-}SCF^+/sKit^-$, 830.4 ± 55.7 vs. $WT\text{-}SCF^-/sKit^-$, 578.6 ± 55.2/mm², $P < 0.05$, $n = 5$; Fig. 6 e) and OC^+ OB density ($WT\text{-}SCF^+/sKit^-$, 495.8 ± 52.2 vs. $WT\text{-}SCF^-/sKit^-$, 350.0 ± 25.8/mm², $P < 0.05$, $n = 5$; Fig. 6 f) around the endochondral ossification area compared with PBS injection (control: $SCF^-/sKit^-$) in WT mice, and the effect of SCF on the increase of capillary density ($WT\text{-}SCF^+/sKit^+$, 601.8 ± 60.0 vs. $WT\text{-}SCF^+/sKit^-$,

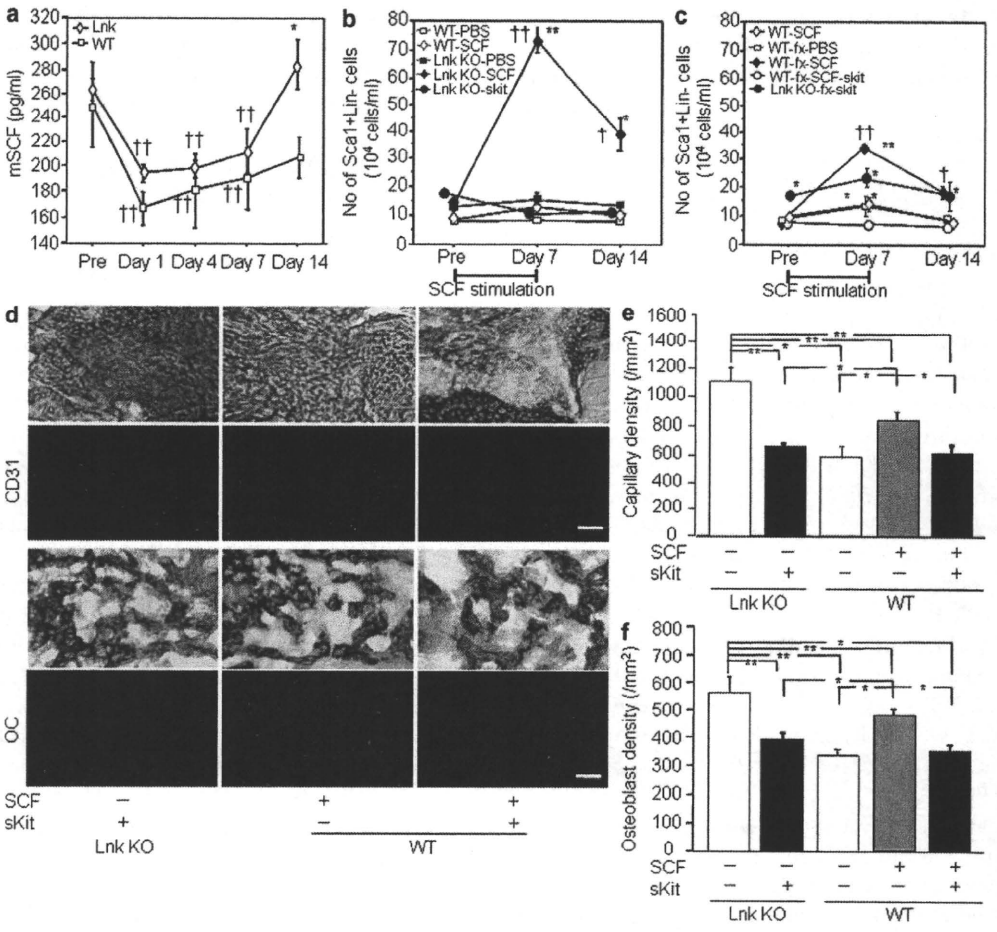

Figure 6. Enhanced SL cell mobilization by SCF stimulation in Lnk KO mice. (a) Serum mouse SCF levels were measured in Lnk KO and WT mice after fracture by ELISA. ††, $P < 0.01$; *, $P < 0.05$ versus Pre, respectively. (b) The number of circulating SL cells in Lnk KO and WT mice with injection of PBS (control; Lnk KO-PBS and WT-PBS), SCF (SCF, 20 μg/kg; Lnk KO-SCF and WT-SCF), or soluble SCF receptor (=c-kit ligand, sKit, 20 μg/kg; Lnk-sKit) were assessed by FACS in the indicated time course after the treatment. †† and †, $P < 0.01$ and $P < 0.05$ versus Pre, respectively. ** and *, $P < 0.01$ and $P < 0.05$ versus WT-PBS, WT-SCF, Lnk KO-PBS, and Lnk KO-sKit, respectively. (c) The number of circulating SL cells in WT mice with fracture and injection of PBS, SCF (20 μg/kg), or SCF (20 μg/kg)+ sKit (WT-fx-PBS, WT-fx-SCF, or WT-fx-SCF-sKit, respectively), WT mice without fracture and SCF (20 μg/kg; WT-SCF), and Lnk KO mice with fracture and sKit (Lnk KO-fx-sKit) were assessed by FACS in the indicated time course after the treatment. †† and †, $P < 0.01$ and $P < 0.05$ versus Pre, respectively. * and **, $P < 0.05$ and $P < 0.01$ versus WT-fx-SCF-sKit, respectively. (d) Immunofluorescent staining for CD31 (green) and OC (OC, green) were performed in granulation tissue samples of peri-fracture sites in Lnk KO (left one panel) and WT (right two panels) mice 7 d after fracture. Alcian blue/orange G stained sections were also shown in parallel with immunostained sections (lower panels to each immunofluorescent staining images). Mouse phenotype with SCF (20 μg/kg) or sKit (20 μg/kg) administration (+) is indicated in the lower part of images. Dotted line indicates bone surface. Bar = 50 μm. Quantification of capillaries (e) and OBs (f). CD31 positive capillaries and OC positive OBs were counted in 3 randomly selected high power fields and averaged.**, $P < 0.01$ and *, $P < 0.05$. All data averaged with SEM from five independent experiments. All experiments were obtained from triplicated assays.

830.4 ± 55.7/mm², P < 0.05, *n* = 5; Fig. 6 e) and OB density (WT-SCF⁺/sKit⁺, 344.6 ± 20.7 vs. WT-SCF⁺/sKit⁻, 495.8 ± 52.2/mm², P < 0.05, *n* = 5; Fig. 6 f) was significantly reversed by coadministration of sKit with SCF. The sKit administration also significantly reduced both capillary density (Lnk KO-SCF⁻/sKit⁺, 653.6 ± 20.4 vs. Lnk KO-SCF⁻/sKit⁻, 1,101.8 ± 97.7/mm², P < 0.01, *n* = 5; Fig. 6 e) and OB density (Lnk KO-SCF⁻/sKit⁺, 389.3 ± 17.3 vs. Lnk KO-SCF⁻/sKit⁻, 558.9 ± 37.9/mm², P < 0.01, *n* = 5; Fig. 6 f) in Lnk KO mice to levels similar to those found in WT mice with or without coadministration of SCF and sKit. These findings indicate that enhanced SL cell mobilization into PB and its recruitment to fracture sites in Lnk KO mice is, at least in part, regulated by SCF–cKit signaling pathway.

SCF–cKit signaling-dependent terminal differentiation of Lnk-deficient OBs for osteogenesis

Although there is no doubt about stimulated stem/progenitor cell recruitment to sites of fracture by SCF–cKit signaling activation in WT and Lnk KO mice, the Lnk-regulated differential potential of progenitors needed to be evaluated, especially regarding osteogenesis. We isolated mouse calvarial OBs from 3–5-d-old Lnk KO mice and WT mice, and compared the differentiation capacity in osteogenic condition medium after 7, 14, and 21 d in culture. Alkaline phosphatase (ALP) staining exhibited larger nodule formation in Lnk KO OBs than in WT OBs until day 14 (Fig. 7 a). In addition, OB mineralized matrix formation assessed by alizarin red staining in Lnk KO OBs was striking compared to that in WT OBs (Fig. 7 a). Quantitative analysis for calcium content in culture medium was also significantly high in Lnk KO OBs than that in WT OBs after 21 d in culture, (Lnk KO-SCF⁻/sKit⁻, 15.9 ± 3.5 vs. WT-SCF⁻/sKit⁻, 0.6± 0.1 mg/ml, P < 0.01, *n* = 5; Fig. 7 d). However, the number of OB CFUs (CFU-O) showed no statistical differences between the two groups at each time point (unpublished data).

Next, we investigated whether this enhancement of differentiation and mineralized matrix formation in Lnk KO OBs was also regulated by SCF signals. First, we confirmed the significantly higher mRNA expression of SCF in Lnk KO mice than that in WT OBs by real-time RT-PCR analysis (Lnk KO, 1.707 ± 0.345 vs. WT, 0.587 ± 0.111, P < 0.05, *n* = 3; Fig. 7 b). In WT mice, as we expected, SCF morphologically enhanced mineralized matrix formation after 21 d in culture (WT-SCF⁺/sKit⁻), and the effect of SCF on WT OBs (WT-SCF⁺/sKit⁺) and Lnk KO OBs (Lnk KO-SCF⁻/sKit⁺) was inhibited by sKit (Fig. 7 c). Calcium content in WT OBs with SCF was significantly higher than that in WT OBs without SCF (WT-SCF⁺/sKit⁻, 7.1 ± 1.4 vs. WT-SCF⁻/sKit⁻, 0.6± 0.1 mg/ml, P < 0.05, *n* = 5), and the effect was reversed by coincubation of SCF and sKit in WT OBs (WT-SCF⁺/sKit⁻, 1.0 ± 0.3 vs. WT-SCF⁺/sKit⁻, 7.1 ± 1.4 mg/ml, P < 0.05, *n* = 5) and in Lnk KO OBs (Lnk KO-SCF⁻/sKit⁺, 4.8 ± 1.1 vs. Lnk KO-SCF⁻/sKit⁻, 15.9 ± 3.5 mg/ml, P < 0.01, *n* = 5; Fig. 7 d). We then further investigated the role of SCF–cKit signaling, focusing on an osteogenesis-related key molecule, bone morphogenetic protein (BMP)-2, was examined in Lnk KO OBs and WT OBs with SCF stimulation in the presence or absence of sKit. The significantly high BMP-2 mRNA expression was observed in Lnk KO OBs and SCF-treated WT OBs compared with WT OBs (Lnk KO-SCF⁻/sKit⁻, 2.732 ± 0.551 and WT-SCF⁺/skit⁻, 2.576 ± 0.369 vs. WT-SCF⁻/skit⁻, 1.189 ± 0.161, P < 0.01, *n* = 3 in each group) and the BMP-2 mRNA up-regulation in Lnk KO OBs and that in SCF-treated WT OBs were significantly inhibited by sKit (Lnk KO-SCF⁻/sKit⁺, 1.391 ± 0.203 vs. Lnk KO-SCF⁻/sKit⁻, 2.732 ± 0.551 and WT-SCF⁻/sKit⁺, 0.911 ± 0.136 vs. WT-SCF⁺/skit⁻, 2.576 ± 0.369, P < 0.01, *n* = 3; Fig. 7 e). These results indicate that BMP-2 might be involved in the SCF–cKit signaling pathway, which is critical for OB terminal differentiation and mineralized matrix formation leading to osteogenesis enhancement in Lnk KO mice.

Lnk gene deficiency in BM cells plays a critical role for fracture healing

Finally, we examined whether Lnk gene deficiency in BM stem/progenitor cells, but not in bone with surrounding tissue. To test this hypothesis, we assessed fracture healing in a murine BMT model. BM cells isolated from either Lnk KO mice or WT mice were transplanted to Lnk KO mice after lethal irradiation, and generated the following chimera mice: 1) Lnk KO mice with Lnk KO BM and 2) Lnk KO mice with WT BM. These chimera mice underwent surgery for fracture and evaluated the fracture healing by micro-CT imaging system and biomechanical analysis 28 d after surgery. The results of micro-CT exhibited striking trabecular bone formation in Lnk KO mice with Lnk KO BM than that in Lnk KO mice with WT BM (Fig. 8 a). Quantitative analysis for bone formation was performed with micro-CT images, and expressed as bone density (Fig. 8 b, left) and trabecula number (Fig. 8 b, right). The both parameters were significantly great in Lnk KO mice with Lnk KO BM compared with that in Lnk KO mice with WT BM (Bone density: Lnk KO mice with Lnk KO BM, 11.3 ± 0.4 vs. Lnk KO mice with WT BM, 8.9 ± 0.8, P < 0.05, *n* = 4 and Number of trabecular: Lnk KO mice with Lnk KO BM, 3.0 ± 0.2 vs. Lnk KO mice with WT BM, 1.8 ± 0.1, P < 0.05, *n* = 4). Biomechanical examinations by three-point bending test also showed significantly increased ultimate stress ratio (Lnk KO mice with Lnk KO BM, 1.1 ± 0.05 vs. Lnk KO mice with WT BM, 0.5 ± 0.08, P < 0.05, *n* = 4), failure energy ratio (Lnk KO mice with Lnk KO BM, 3.9 ± 0.07 vs. Lnk KO mice with WT BM, 1.5 ± 0.05, p<,0.001 *n* = 4), and extrinsic stiffness ratio (Lnk KO mice with Lnk KO BM, 0.8 ± 0.03 vs. Lnk KO mice with WT BM, 0.2 ± 0.03, P < 0.05, *n* = 4; Fig. 8 c). These results suggest that Lnk gene deficiency in BM cells, rather than in bone with surrounding tissue, is critical for enhanced fracture healing.

DISCUSSION

In this paper, we have demonstrated that both vasculogenesis and osteogenesis were enhanced via large-scale HSC/EPC mobilization in circulation and recruitment to sites of fracture,

Published September 20, 2010

simultaneously resulting in accelerated bone healing in a Lnk-deficient mouse fracture model.

BM SL cells, recognized as an HSC/EPC-enriched fraction (Takahashi et al., 1999), were reported to synthesize ALP, collagen, and OC and form a mineralized matrix in culture over a decade ago (Van Vlasselaer et al., 1994). It has also been reported that BM side population cells, which contain hematopoietic repopulating cells, can also engraft in bone after transplantation (Dominici et al., 2004), and that the nonadherent population of BM cells contains primitive cells able to generate both hematopoietic and osteocytic lineage cells (Olmsted-Davis et al., 2003). Zhang et al. (2003) reported that depleting a receptor of BMP in OBs caused a doubling in both OB and HSC populations in BM niche. Calvi et al. (2003) also found a parallel expansion of the HSCs when the number of OBs was increased by parathyroid hormone infusion. These findings indicate that osteogenesis and hematopoiesis/vasculogenesis closely regulated each other in terms of

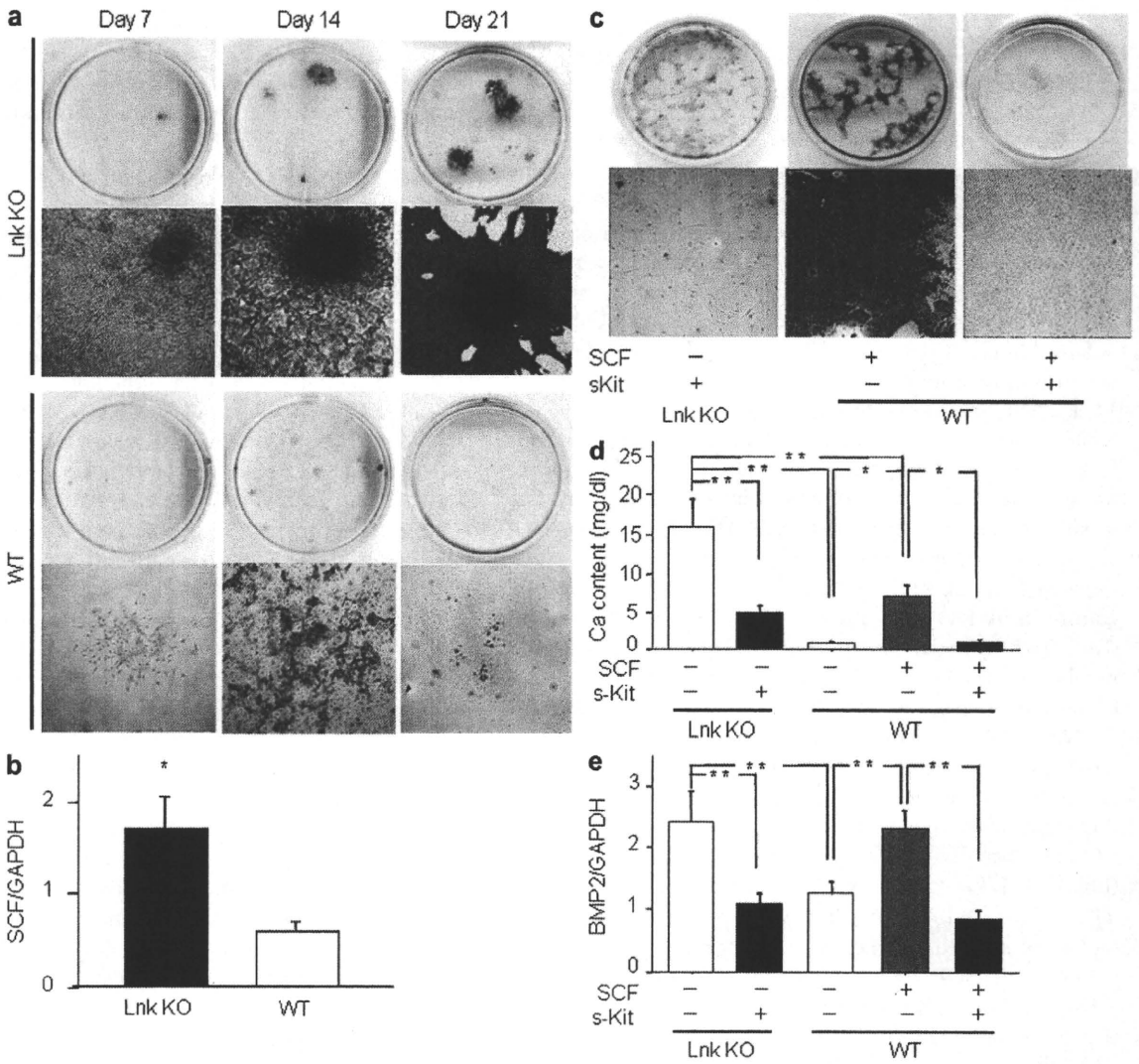

Figure 7. Enhanced mineralization of OBs in Lnk-deficient mice. (a) OBs (OBs) isolated from Lnk KO and WT mice were cultured in osteogenic condition medium. Cells were assessed morphologically by ALP staining (blue) at day 14 and by alizarin red staining (red) at day 21. Upper panels show macroscopic images of whole culture dishes and lower panels show magnified images of nodule with mineralized matrix formation. (b) Real-time RT-PCR of cultured OBs for SCF mRNA expression at day 7 in Lnk KO and WT mice. Mouse heart and bone are used as positive controls for mouse endothelial and bone-related gene detection (not depicted) *, $P < 0.05$. Data averaged with SEM from three independent experiments. Experiments were obtained from triplicated assays. (c) The mineralized matrix formation was assessed by alizarin red staining 21 d after osteogenic culture in Lnk KO OBs with sKit (10 µg/ml) and in WT OBs in the presence of SCF (100ng/ml) with or without sKit (10 µg/ml). Upper panels show macroscopic images of whole culture dishes and lower panels show magnified images of nodule with mineralized matrix formation. Calcium content was measured by ELISA ($n = 5$ each; d) in culture medium and BMP2 mRNA expression (e) was analyzed by real-time RT-PCR ($n = 3$ each) in Lnk KO OBs with sKit (10 µg/ml) and WT OBs in the presence of SCF (100ng/ml) with or without sKit (10 µg/ml). *, $P < 0.05$ and **, $P < 0.01$. Experiments were obtained from triplicated assays.

Published September 20, 2010

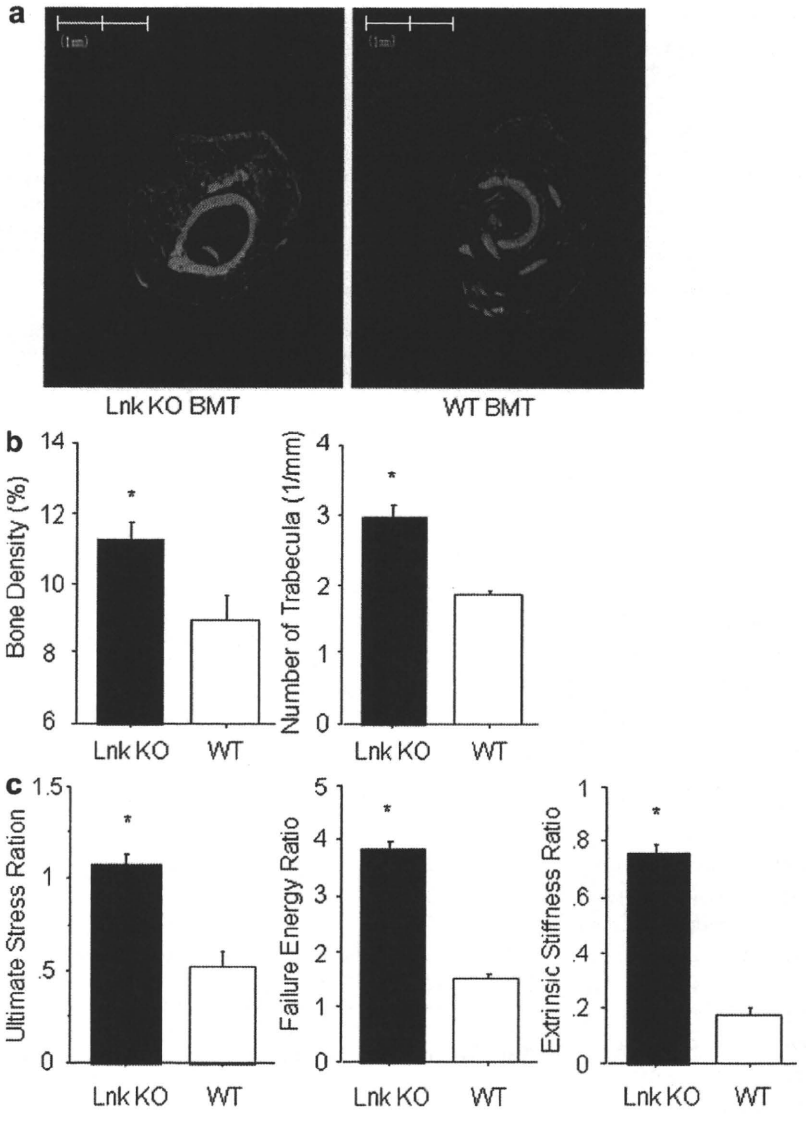

Figure 8. Radiographical and biomechanical function assessment of fracture healing in Lnk KO BMT–Lnk KO mice and WT BMT– Lnk KO mice. (a) The bone structure after healing was assessed by micro-CT 28 d after surgery. (b), Bone density and number of trabecular bones were quantified in the micro-CT images and averaged. *, $P < 0.05$ versus Lnk KO-BMT, $n = 4$ each. (c) Biomechanical function test for healed bone was also assessed 28 d after fracture. Each parameter, ultimate stress (left), fracture energy (center) and extrinsic stiffness ratio (right), was evaluated as healed bone function. *, $P < 0.05$ and **, $P < 0.001$ versus Lnk KO-BMT. All data averaged with SEM from four independent experiments.

microenvironmental interaction for regenerative activity in BM. We have also previously reported that mobilization of BM-derived HSCs/EPCs were triggered by fracture onset and recruited to sites of fracture (Matsumoto et al., 2008). In this study, we have provided evidence of enhanced translineage differentiation of $Sca1^+/Tie2^+$ cells into OBs and ECs both in vitro and in vivo, as well as that of mobilization of BM-KSL cells and PB-SL cells in circulation in Lnk-deficient mice, which is consistent with the previous report that BM cells of Lnk-deficient mice are competitively superior in hematopoietic population to those of WT mice (Takaki et al., 2002). These data suggest that a large number of BM-derived EPCs might not only be mobilized from BM but also recruited to fracture site, differentiating into ECs and OBs by lack of Lnk signaling. In addition to the direct contribution of recruited EPCs for fracture repair, indirect contribution of EPCs, i.e., the paracrine effect on bone tissue regeneration via promotion of osteogenesis/angiogenesis with resident cells, would also be critical for fracture healing (Matsumoto et al., 2006). Indeed, cDNA microarray and quantitative real-time RT-PCR analyses also exhibited up-regulation of pro-angiogenic/-osteogenic gene expressions, which is consistent with increased blood perfusion and callus formation, in sites of fracture with recruited EPCs in Lnk-deficient mice. The series of findings suggest that both direct and indirect contribution of BM-derived EPCs to prompt and functional fracture healing with sufficient mineralization in Lnk-deficient mice.

Takaki et al. (2000, 2002) reported that Lnk acts as a negative regulator in the SCF–cKit signaling pathway. Although the role of Lnk system has gradually been clarified in the field of hematology, nothing is known about it's role in skeletal biology and bone regeneration and repair. Here, we have provided evidence that enhanced HSC/EPC mobilization into PB and its recruitment to the fracture site in Lnk-deficient mice are regulated, at least in part, by SCF–cKit signaling pathway, which was proved by gain and loss of function test using SCF and sKit. However, enhanced vasculogenesis and osteogenesis in Lnk-deficient mice was shown to be significantly superior to that of SCF-treated WT mice, suggesting that another mechanism besides SCF–cKit signaling pathway is involved in the Lnk signal lacking accelerated bone healing. Indeed, molecular cDNA array analysis showed that BMPR2 mRNA expression was up-regulated more in Lnk KO mice than in WT mice. Moreover, lack of Lnk or SCF supplement in OBs induced terminal differentiation and mineralized matrix formation with increased BMP2 gene expression, which was blocked by the SCF antagonist sKit. These findings are consistent with previous studies in which cKit expression is shown in OBs and P-2 enhances OB differentiation. (Bilbe et al., 1996; Hassel et al., 2006) Collectively, it is suggested that OB differentiation and maturation is enhanced in Lnk-deficient mice via the mechanism of BMP2-involved SCF–cKit signaling pathway.

Published September 20, 2010

Another interesting finding in cDNA microarray data is that expression of vascular cell adhesion molecule (VCAM)-1, a differentiation-predicting marker for osteogenesis (Fukiage et al., 2008), is significantly up-regulated in sites of fracture and EC-related markers in Lnk KO mice compared with WT mice. Fitau et al. (2006) reported that high expression of VCAM-1 at both the mRNA and protein level in Lnk-deficient mice was regulated in TNF-treated ECs by extracellular signal-related kinase (Erk) 1/2 pathways. In addition, Rhee et al. (2006) reported that Erk 1/2 expression was present within mesenchymal precursor cells during distraction osteogenesis and that Erk expression closely correlates with BMP 2/4 expression. Other studies also indicated that the activation of Erk 1/2 pathway in OBs related to mechanical strain and fluid flow (Jessop et al., 2002; Alford et al., 2003; Liu et al., 2008). Based on this evidence and our findings, the Erk1/2- and BMP-2/4–involved VCAM-1 signaling pathway is considered to be another mechanism for accelerated fracture healing via vasculogenesis and osteogenesis in Lnk KO mice, and further investigation will be required to clarify the entire mechanism for bone regeneration in a Lnk-deficient system.

In conclusion, our data provide novel evidence that the Lnk system acts as a negative regulator in the SCF–c-Kit signaling pathway and that Lnk deficiency modulates both vasculogenesis and osteogenesis via SL stem cell mobilization in PB and $Tie2^+$ BM cell recruitment to sites of fracture, although $Tie2^+$ cells are not necessarily defined as stem cells, but are likely EPCs. In addition, lack of Lnk signaling further enhances BMP2-induced OB matrix mineralization in vitro. These pathophysiological changes led to accelerated bone healing in Lnk-deficient mice. In the field of skeletal regeneration, recently BM-derived mesenchymal stem cells or whole BMs have been used for injured bone (Petite et al., 2000) or osteogenesis imperfecta (Horwitz et al., 1999) in preclinical studies. However, there are several issues to be resolved for open reduction, such as invasiveness in cell transplantation procedure and possible complications caused by infection. The major strength of this study relies on the concept that negative control of Lnk system for bone regeneration leads to clinical feasibility by generating a Lnk-inhibitory compound. This is the first study demonstrating physiological functions of the adaptor protein Lnk in bone regeneration and suggests that inhibition of the Lnk system could be a novel therapeutic application for genetic bone diseases and bone injuries.

MATERIALS AND METHODS

Mice. $Lnk^{-/-}$ mice, whose generation and genomic cloning were described previously (Takaki et al., 2000) were backcrossed with C57BL/6 (B6-Ly5.2) >10 times and paired with age-matched WT mice as controls. Mice congenic for the Ly5 locus (B6-Ly5.1) were bred and maintained at the animal facility of Institute of Physical and Chemical Research Center for Developmental Biology, Kobe, Japan. The mice were fed a standard maintenance diet and provided water ad libitum. Male 10–12-wk-old $Lnk^{-/-}$ and WT mice were used in this study. The institutional animal care and use committees of the Institute of Physical and Chemical Research Center for Developmental Biology approved all animal procedures, including human cell transplantation.

Isolation of Lin^- BM cells. To confirm the kinetics of KSL or SL cells in BM and PB, we detected KSL or SL cells at pre-fracture and 1, 4, 7, and 14 d post-fracture by FACS analysis ($n = 3$ at each day).

BM cells were obtained by flushing femurs and tibiae or PB cells were aspirated from the hearts of 10-wk-old Lnk KO mice or WT mice with PBS containing 5% FCS. MNCs were obtained by gradient separation onto a Ficoll Histopaque gradient. Separation of Lin^- cells was performed by labeling MNCs with a lin^- separation kit (BD) containing biotin-conjugated Mac1, B220, CD3e, Ter119, Ly6G, and CD45R antibodies, followed by streptavidin-conjugated magnetic beads and BD IMagnet separation before Lin^- MNCs were counted.

Multilineage differentiation culture of SL BM cells. Mouse SL cells were isolated from BM MNCs by Lin^+ cell depletion with MACS system (Miltenyi Biotec) followed by FACS system with an anti–mouse Sca-1 antibody (FACSAria; BD), and cultured in α-modified Eagle's medium (α-MEM; Cambrex Bio Science). After 3 wk in culture, cells (10^5/well) were placed in a 6-well plate and further cultured only for osteogenic and adipogenic induction.

For endothelial induction, freshly isolated SL cells were cultured in EBM-2 medium supplemented with 10% FBS and EGM-2 Bullet kit (Lonza) in Pronectin F (Sanyo Chemical, Inc.)–coated culture plate for 7 d. For osteogenic and adipogenic induction, cells were cultured in α-MEM supplemented with 10% FBS. 2 mM L-glutamine, 60 μM ascorbic acid, 10 mM β-glycerophosphate and 0.1 μM dexamethasone (Sigma-Aldrich) and α-MEM supplemented with 1 μM dexamethasone, 60 μM indomethacin, and 5 μg/ml insulin (Sigma-Aldrich) for 3 wk, respectively. After the above induction cultures, each lineage differentiation was confirmed by real-time RT-PCR and fluorescent immunocytostaining for the indicated specific markers. Also, calcium deposits were detected by Alizarin red staining and formations of lipid droplets were assessed by Oil Red O staining as characteristics of OB and AD, respectively. Freshly isolated SL cells and those cultured for 3 wk in α-MEM alone were used as controls for endothelial induction and osteogenic/adipogenic induction in real-time RT-PCR analysis, respectively.

Flow cytometry studies and monoclonal antibodies. Regular flow cytometric profiles were analyzed with a FACSCalibur analyzer and CELLQuest software (BD). The instrument was aligned and calibrated daily using a four color mixture of CaliBRITE beads (BD) with FACSComp software (BD). Dead cells were excluded from the plots beads on propidium iodide (PI) staining (Sigma-Aldrich). Lineage-depleted MNCs were washed twice with HBSS containing 3.0% heat-activated FCS, and incubated with 10 μl of FcR Blocking Regent to increase the specificity of monoclonal antibodies (Miltenyi Biotec) for 20 min at 4°C, and incubated with the monoclonal antibodies for 30 min at 4°C. The stained cells were washed three times with PBS containing 3.0% FCS, and resuspended in 0.5 ml of HBSS/3%FCS/PI, and analyzed by FACScan caliber flow cytometer (BD). The following monoclonal antibodies were used to characterize the lineage-depleted MNCs: APC-conjugated anti-cKit (BD), FITC-conjugated anti-Sca1 (BD), IgG1-PE isotype controls (BD), IgG1-FITC isotype controls (BD), and PI (Sigma-Aldrich).

Induction of femoral fracture. All surgical procedures were performed under anesthesia and normal sterile conditions. Anesthesia was performed with ketamine hydrochloride (60 mg/kg) and xylazine hydrochloride (10 mg/kg) administered intraperitoneally. We followed Manigrasso's model of closed femur fracture (Manigrasso and O'Connor, 2004). A lateral parapatellar knee incision on the right limb was made to expose the distal femoral condyle. A 2-mm wedge was made using a 27-gauge needle on the intercondyle of the femur and then a 0.5-mm-diam, stainless wire was inserted in a retrograde fashion. The wire was advanced until its proximal end was positioned stable to the greater trochanter and the distal end was cut close to the articular surface of the knee. A transverse femoral shaft fracture was then created in the right femur of each mouse by three-point bending. The wound was then irrigated with 10 cc of sterile saline and skin was closed in layers with 5–0

Published September 20, 2010

nylon sutures. Postoperative pain was managed by administration of subcutaneous injection of buprenorphine hydrochloride after surgery. Unprotected weight bearing was allowed immediately after the operation. The left nonfractured femur served as a control.

20 animals were assigned to each group for radiological assessment, and every additional three to five animals in each group were assigned for each study. If the fracture produced was not a stable transverse fracture or if evidence of deep infection developed then animals were excluded from the study and replaced with another animal. Thus, six mice with comminuted fractures were replaced during the experiment. No mice developed infections, as confirmed by radiograph.

Mouse BMT model. Male Lnk KO mice and WT mice (C57BL6/J; CLEA Japan, Inc.) aged 6 wk were used as recipients for BMT. Transgenic mice of B6/N-TgN (Tie-2-LacZ)^{182Sato} (Jackson ImmunoResearch Laboratories), which were generated by backcrossing FVB/N-TgN (Tie-2-LacZ)^{182Sato} mice and C56BL6/J mice, were used as donors for the BMT. The procedure of BMT was performed as described previously, with some modifications (Ii et al., 2005). In brief, the recipient mice were lethally irradiated for BM ablation with 12.0 Gy and received 5 million donor BM MNCs. At 4–6 wk after BMT, by which time the BM of the recipient mice was reconstituted, surgery for fracture induction was performed. The granulation tissue of fractured BMT mice were harvested 7 and 28 d after surgery for histological, radiographical, and biomechanical function analyses.

Gene expression analysis via cDNA microarray. Total RNA was obtained from tissues at the peri-fracture site at day 7 using Tri-zol (Life Technologies) according to the manufacturer's instructions. cDNAs were synthesized using 1 μg total RNA in the presence of Superscript II and Oligo $(dT)_{1218}$ (both from Invitrogen). PCR was performed in a 20-μl reaction solution containing 2 μl 10 X PCR buffer, 150 nmol $MgCl_2$, 10 nmol dNTP, 20 pmol primer, 1 μl 10× diluted cDNA, and 1 U RedTag DNA polymerase (Sigma-Aldrich). PCRs were run as follows: 35 cycles of 94°C for 30 s, 55°C for 30 s and 72°C for 30 s, and a final extension for 10 min at 72°C. Primer sequences are shown in the Primer size and sequence section. Nonradioactive GEArray Q series cDNA expression array filters (Mouse Angiogenesis Gene Array [MM-009] and Mouse Osteogenesis Gene Array [MM-026]; SuperArray Inc.) were used to perform focused array analysis as described by the manufacturer. Microarray databases are available at the National Center for Biotechnology Information Gene Expression Omnibus (GEO; http://www.ncbi.nlm.nih.gov/geo/) under accession no. GPL1121 for MM-009 and GPL1143 for MM-026. In brief, biotin dUTP-labeled cDNA probes were generated in the presence of a designed set of gene-specific primers using total RNA (2 μg per filter) and 200 U MMLV reverse transcription (Promega, Madison, WI, USA). The array filters were hybridized with biotin-labeled probes at 60°C for 17 h. Filters were first washed twice with 2× saline sodium citrate buffer (SSC)/1% sodium dodecyl sulfate (SDS) and then twice with 0.1× SSC/1% SDS at 60°C for 15 min each. Chemiluminescent detection steps were performed by subsequent incubation of the filters with ALP-conjugated streptavidin and CDP-Star substrate. The images were captured using ChemoFlure 8900 (Alpha Innotech). For data analysis, positive and negative spots were independently identified and verified by at least two people. Only matched positive and negative results from two independent experiments were used for analysis. For quantification, intensity of spots was first measured by National Institutes of Health image software (ImageJ) and then the mean intensities derived from the blank spots were subtracted. These subtracted intensities were divided by the mean intensities from GAPDH (three spots in each array), to obtain a relative intensity for each spot. These relative intensities were used to compare gene express levels between the control and the stimulated groups.

Real-time quantitative RT-PCR analysis of RNA isolated from peri-fracture site and cultured OBs. Total RNA was obtained from tissues of peri-fracture site at day 7 or from cultured OBs using TRIzol (Life Technologies) according to the manufacturer's instructions. After total RNA isolation, we made single-strand cDNA using a reverse transcription kit (Invitrogen) and used it as template for real-time PCR with SYBR Green PCR Master Mix (Applied Biosystems) and gene-specific primers in an Oligo software (Takara Bio Inc.). The mean cycle threshold values from quadruplicate measurements were used to calculate the gene expression, with normalization to GAPDH as an internal control.

Primer size and sequences. mCD31 (224 bp): sense 5′-TCCCCACCGAAAGCAGTAAT-3′; antisense 5′-CCCACGGAGAAGTACTCTGTCTATC-3′, mVE-cad (369 bp): sense 5′-GAGCTAAGAGGACCCTCTGCTACTC-3′; antisense 5′-TGGGCCTCTTTGTGTCTGTATG-3′, mFlk-1 (346 bp): sense 5′-TGGCGTTTCCTACTCCTAATGA-3′; antisense 5′-GAAGCCACAACAAAGCTAAAATACTGAG-3′, mvWF (20 bp): sense 5′-ACGCCATCTCCAGATTCAAG-3′; antisense 5′-AAGCATCTCCCACAGCATTC-3′, mOC (187 bp): sense 5′-CTGACCTCACAGATCCCAAGC-3′; antisense 5′-TGGTCTGATAGCTCGTCACAA-3′, mCol1A1 (107 bp): sense 5′-CAATGGTGAGACGTGGAAAC-3′; antisense 5′-GGTTGGGACAGTCCAGTTCT-3′, mCbfa1 (151 bp): sense 5′-AACGATCTGAGATTTGTGGGC-3′; antisense 5′-CCTGCGTGGGATTTCTTGGTT-3′, mLPL (65 bp): sense 5′-AGCTGGGAGCAGAAACTGTG-3′; antisense 5′-CATGTGGGTTGGTGTTCAGA-3′, mPPARγ (50 bp): sense 5′-CTGGCCTCCCTGATGAATAA-3′; antisense 5′-AATCCTTGGCCCTCTGAGAT-3′, mSCF (72 bp): sense 5′-CCAAAAGCAAAGCCAATTACAAG-3′; antisense 5′-AGACTCGGGCCTACAATGGA-3′, mBMP-2 (73 bp): sense 5′-TCACTTATAGCCGCATTATCTTCTTC-3′; antisense 5′-TTGGTTTATCCATGAGGCTAACTG-3′, and mGAPDH (484 bp): sense 5′-GTGAGGCCGGTGCTGAGTATG-3′; antisense 5′-AGGCGGCACGTCAGATCC-3′.

Tissue harvesting. Mice were euthanized with an overdose of ketamine and xylazine. Bilateral femurs were harvested and embedded in OCT compound, snap frozen in liquid nitrogen, and stored at −80°C for histochemical staining and immunohistochemistry. Rat femurs in OCT blocks were sectioned, and 6-μm serial sections were collected on slides, followed by fixation with 4.0% paraformaldehyde at 4°C for 5 min, and then stained immediately.

Morphometric evaluation of capillary and OB density. Immunohistochemical staining with anti–mouse rat CD31 (Biogenesis) for mouse EC marker or anti–mouse goat OC (Santa Cruz Biotechnology, Inc.) for mouse OB was performed. The secondary antibodies for each immunostaining are as follows: FITC-conjugated anti–rat IgG (H+L; Jackson ImmunoResearch Laboratories) for CD31 and FITC-conjugated anti–goat IgG (H+L; Jackson ImmunoResearch Laboratories) for OC. Capillary or OB density was morphometrically evaluated by histological examination of 5 randomly selected fields of tissue sections recovered from segments of soft tissue in the peri-fracture site. Capillaries were recognized as tubular structures positive for CD31. OB-like cells were recognized as lining or floating cells positive for OC on new bone surface. All morphometric studies were performed by two examiners who were blinded to treatment.

LDPI assessment. LDPI (Moor Instrument; Wardell et al., 1993; Linden et al., 1995) was used to record serial blood flow measurements over the 3 wk post-fracture course. In these digital color-coded images, red hue indicated regions with maximum perfusion; medium perfusion values are shown in yellow; lowest perfusion values are represented as blue. This was done under anesthesia with the animal supine and both limbs fully fixed.

Fluorescent immunostaining. To detect $Tie2^+$ cell-derived neovascularization in Lnk KO mice with Tie2/LacZ Lnk KO BM at the fracture site, double immunohistochemistry was performed with anti–mouse rat CD31 (1:50; BD) or anti–mouse goat OC (1:250; Biogenesis) and anti–rabbit β-gal (1:1,000; Cortex) to detect $Tie2^+$ cell-derived ECs or OBs. For characterization of multilineage cell types in SL cells, the following primary antibodies were used: anti–mouse rat CD31 (1:50; BD), anti–mouse goat vWF (1:100; Santa Cruz Biotechnology, Inc.), anti–mouse rat Flk-1 (1:100; Chemicon), anti–mouse goat OC (1:250; Biogenesis), and anti–mouse mouse adiponectin

(1:250; Abcam). The secondary antibodies (1:1,000) for each immunostaining are as follows: FITC-conjugated anti-rat IgG (H+L; Jackson ImmunoResearch Laboratories) for CD31 and Flk-1, FITC-conjugated anti-goat IgG (H+L; Jackson ImmunoResearch Laboratories) for OC and vWF, Alexa Fluor 594–conjugated rabbit anti-mouse IgG (H+L) for adiponectin, and Cy3-conjugated goat anti-rabbit IgG (H+L; Jackson ImmunoResearch Laboratories) for β-gal staining. DAPI solution was applied for 5 min for nuclear staining.

Radiological assessment. Radiographs of the fractured legs were serially taken at weeks 0, 1, 2, 3, and 4 after creation of the fracture. This procedure was done under anesthesia with the animal supine and both limbs fully extended. Fracture union was identified by the presence of bridging callus on two cortices. Radiographs of each animal were examined by three observers who were blinded to treatment. To evaluate the fracture healing process, callus formation was monitored radiographically and relative callus areas detected by radiography were quantified with National Institutes of Health image at week 1 in both groups. To evaluate bone remodeling, callus absorption was monitored radiographically and relative callus density was detected by radiography were quantified with ImageJ at week 3 and 4 in all groups.

For quantification of callus/trabecular bone formation, micro-CT imaging analysis was performed 4 wk after fracture surgery in Kureha Special Laboratory. In brief, bone density and number of trabecula in callus area were calculated with CT intensity in scanned images by single energy x-ray absorptiometry method and averaged.

Biomechanical analysis of fracture union. Biomechanical evaluation was performed with mice at week 4 after fracture in Kureha Special Laboratory. In brief, fractured femurs and the contralateral nonfractured femurs were prepared and intramedullary fixation pins were removed before the bending test. The standardized three-point bending test was performed using load torsion and bending tester "MZ-500S" (Maruto Instrument Co., Ltd.). The bending force was applied with cross-head at a speed of 2 mm/minute until rupture occurred. The ultimate stress (n), the extrinsic stiffness (n/mm) and the failure energy ($n \times$ mm) were interpreted and calculated from the load deflection curve. The relative ratio of the fractured (right) femur to nonfractured (left) femur was calculated in each group and averaged.

Histological assessment. Histological evaluation ($n = 3$ in each group) was performed with toluidine blue staining to address the process of endochondral ossification on weeks 1, 2, and 3. The degree of fracture healing was evaluated at week 1, 2, and 3 in each group using a five point scale proposed by Allen et al. (1980). According to this classification system, grade four represents complete bony union, grade three represents an incomplete bony union (presence of a small amount of cartilage in the callus), grade two represents a complete cartilaginous union (well-formed plate of hyaline cartilage uniting the fragments), grade one represents an incomplete cartilaginous union (retention of fibrous elements in the cartilaginous plate), and grade zero indicates the formation of a pseudoarthrosis (most severe form of arrest in fracture repair). All morphometric studies were performed by two orthopedic surgeons who were blinded to the treatment.

ELISA assessment of plasma SCF levels. SCF plasma levels of mouse were measured at prefracture and 1, 4, 7, and 14 d post-fracture in both groups via ELISA kit (R&D Systems) according to the manufacturer's instructions ($n = 3$ in each group).

Effect of SCF stimulation on mobilization of SL cells. Mice were injected intraperitoneally with 20 μg/kg SCF or PBS for 5 d in un-fractured Lnk KO, WT, and fractured WT mice, and mobilization of SL cells to PB was assessed at prefracture, day 7, and day 14 post-stimulation time point by FACS analysis ($n = 5$ in each group). For the other series, SCF or PBS-treated WT mice of femur fracture model were sacrificed at day 7, and tissue samples of the fractured limbs were assessed by capillary and OB density as mentioned in Morphometric evaluation of capillary and OB density.

Mouse calvarial OB culture. Calvarial cells were isolated from 3–5-d-old mice using a modification of the method described by Wong and Cohn (1975). In brief, after removal of sutures, calvariae were subjected to four sequential 15-min digestions in an enzyme mixture containing 0.05% trypsin (Invitrogen) and 0.1% collagenase P (Boehringer Mannheim) at 37°C on a rocking platform. Cell fractions 2–4 were collected, and enzyme activity was stopped by the addition of an equal volume of DME containing 10% FCS, 100 U/ml of penicillin, and 100 μg/ml of streptomycin (Invitrogen). The fractions were pooled, centrifuged, resuspended in DME containing 10% FCS, and filtered through a 70-μm cell strainer. Cells were plated at a density of 10^4 cells/well in 35-mm culture plates in DME containing 10% FCS. The medium was changed 24 h later, and 3 d later cultures were fed again. At 1 wk of culture, the medium was changed to a differentiation medium (α-MEM containing 10% FCS, 50 μg/ml of ascorbic acid, and 4 mM of β-glycerophosphate) and thereafter the medium was changed every 2 d. CFU-O was scored at day 7, 14, and 21 of incubation by in situ observation of plates on an inverted microscope. Effects of SCF and sKit on CFU-O formation and mineralization were also investigated in the above assay. Purified recombinant human SCF and sKit were purchased from R&D Systems and supplemented concentrations of cytokines used for culture were as follows: SCF 100 ng/ml and sKit 10 μg/ml (Nakamura, 2004).

Histochemical analysis of cell cultures. Histochemical staining for ALP was performed at day 7 and 14 using a commercially available kit (Muto-Kagaku) according to the manufacturer's instruction. Mineralization was assessed using alizarin red staining method. In brief, the cultures were rinsed twice with PBS, fixed in 100% ethanol for 30 min, and stained wth 1% alizarin red S (Hartman Leddon Co.) in 0.28% ammonia water for 10 min at room temperature. The stained cell layers were washed, rinsed twice with distilled water, and air-dried.

Matrix/intracellular calcium accumulation. Calcium content was measured by the orthocresolphthalein complexone (OCPC) colorimetric method (Sigma-Aldrich). In brief, cell layers at day 21 were washed with PBS twice, and then incubated with 50 μl of 0.6 N hydrochloric acid overnight at room temperature. Plates were then vortexed and centrifuged for 20 min at 1,600 g at 25°C and 10 μl of sample was added to 100 μl OCPC solution in fresh wells. The plate was incubated at room temperature for 10 min, and then read at 575 nm. Standards were prepared from a $CaCl_2$ solution and the results were expressed in milligram/milliliter per 10,000 seeded cells.

Statistical analysis. All values were expressed as mean ± SEM. Paired Student's t tests were performed for comparison of data before and after fracture. The comparisons among groups were made using the one-way analysis of variance. Post hoc analysis was performed by Fisher's PLSD test. A p-value < 0.05 was considered to denote statistical significance.

The authors state that there is no conflict of interest.

Submitted: 16 February 2010
Accepted: 30 July 2010

REFERENCES

Ahmed, Z., and T.S. Pillay. 2003. Adapter protein with a pleckstrin homology (PH) and an Src homology 2 (SH2) domain (APS) and SH2-B enhance insulin-receptor autophosphorylation, extracellular-signal-regulated kinase and phosphoinositide 3-kinase-dependent signalling. *Biochem. J.* 371:405–412. doi:10.1042/BJ20021589

Alford, A.I., C.R. Jacobs, and H.J. Donahue. 2003. Oscillating fluid flow regulates gap junction communication in osteocytic MLO-Y4 cells by an ERK1/2 MAP kinase-dependent mechanism small star, filled. *Bone.* 33:64–70. doi:10.1016/S8756-3282(03)00167-4

Allen, H.L., A. Wase, and W.T. Bear. 1980. Indomethacin and aspirin: effect of nonsteroidal anti-inflammatory agents on the rate of fracture repair in the rat. *Acta Orthop. Scand.* 51:595–600. doi:10.3109/17453678008990848

Published September 20, 2010

Asahara, T., T. Murohara, A. Sullivan, M. Silver, R. van der Zee, T. Li, B. Witzenbichler, G. Schatteman, and J.M. Isner. 1997. Isolation of putative progenitor endothelial cells for angiogenesis. *Science*. 275:964–967. doi:10.1126/science.275.5302.964

Bilbe, G., E. Roberts, M. Birch, and D.B. Evans. 1996. PCR phenotyping of cytokines, growth factors and their receptors and bone matrix proteins in human osteoblast-like cell lines. *Bone*. 19:437–445. doi:10.1016/S8756-3282(96)00254-2

Blau, H.M., T.R. Brazelton, and J.M. Weimann. 2001. The evolving concept of a stem cell: entity or function? *Cell*. 105:829–841. doi:10.1016/S0092-8674(01)00409-3

Broudy, V.C. 1997. Stem cell factor and hematopoiesis. *Blood*. 90:1345–1364.

Calvi, L.M., G.B. Adams, K.W. Weibrecht, J.M. Weber, D.P. Olson, M.C. Knight, R.P. Martin, E. Schipani, P. Divieti, F.R. Bringhurst, et al. 2003. Osteoblastic cells regulate the haematopoietic stem cell niche. *Nature*. 425:841–846 (see comment). doi:10.1038/nature02040

Colnot, C. 2009. Skeletal cell fate decisions within periosteum and bone marrow during bone regeneration. *J. Bone Miner. Res.* 24:274–282. doi:10.1359/jbmr.081003

Colnot, C.I., and J.A. Helms. 2001. A molecular analysis of matrix remodeling and angiogenesis during long bone development. *Mech. Dev.* 100:245–250. doi:10.1016/S0925-4773(00)00532-3

Dominici, M., C. Pritchard, J.E. Garlits, T.J. Hofmann, D.A. Persons, and E.M. Horwitz. 2004. Hematopoietic cells and osteoblasts are derived from a common marrow progenitor after bone marrow transplantation. *Proc. Natl. Acad. Sci. USA*. 101:11761–11766. doi:10.1073/pnas.0404626101

Ema, H., K. Sudo, J. Seita, A. Matsubara, Y. Morita, M. Osawa, K. Takatsu, S. Takaki, and H. Nakauchi. 2005. Quantification of self-renewal capacity in single hematopoietic stem cells from normal and Lnk-deficient mice. *Dev. Cell*. 8:907–914. doi:10.1016/j.devcel.2005.03.019

Fitau, J., G. Boulday, F. Coulon, T. Quillard, and B. Charreau. 2006. The adaptor molecule Lnk negatively regulates tumor necrosis factor-alpha-dependent VCAM-1 expression in endothelial cells through inhibition of the ERK1 and -2 pathways. *J. Biol. Chem.* 281:20148–20159. doi:10.1074/jbc.M510997200

Fukiage, K., T. Aoyama, K.R. Shibata, S. Otsuka, M. Furu, Y. Kohno, K. Ito, Y. Jin, S. Fujita, S. Fujibayashi, et al. 2008. Expression of vascular cell adhesion molecule-1 indicates the differentiation potential of human bone marrow stromal cells. *Biochem. Biophys. Res. Commun.* 365:406–412. doi:10.1016/j.bbrc.2007.10.149

Harper, J., and M. Kalgsbrun. 1999. Cartilage to bone–angiogenesis leads the way. *Nat. Med.* 5:617–618. doi:10.1038/9460

Hassel, S., M. Yakymovych, U. Hellman, L. Ronnstrand, P. Knaus, and S. Souchelnytskyi. 2006. Interaction and functional cooperation between the serine/threonine kinase bone morphogenetic protein type II receptor with the tyrosine kinase stem cell factor receptor. *J. Cell. Physiol.* 206:457–467. doi:10.1002/jcp.20480

Horwitz, E.M., D.J. Prockop, L.A. Fitzpatrick, W.W. Koo, P.L. Gordon, M. Neel, M. Sussman, P. Orchard, J.C. Marx, R.E. Pyeritz, and M.K. Brenner. 1999. Transplantability and therapeutic effects of bone marrow-derived mesenchymal cells in children with osteogenesis imperfecta. *Nat. Med.* 5:309–313 (see comment). doi:10.1038/6529

Huang, X., Y. Li, K. Tanaka, K.G. Moore, and J.I. Hayashi. 1995. Cloning and characterization of Lnk, a signal transduction protein that links T-cell receptor activation signal to phospholipase C gamma 1, Grb2, and phosphatidylinositol 3-kinase. *Proc. Natl. Acad. Sci. USA*. 92:11618–11622. doi:10.1073/pnas.92.25.11618

Ii, M., H. Nishimura, A. Iwakura, A. Wecker, E. Eaton, T. Asahara, and D.W. Losordo. 2005. Endothelial progenitor cells are rapidly recruited to myocardium and mediate protective effect of ischemic preconditioning via "imported" nitric oxide synthase activity. *Circulation*. 111:1114–1120. doi:10.1161/01.CIR.0000157144.24888.7E

Jessop, H.L., S.C. Rawlinson, A.A. Pitsillides, and L.E. Lanyon. 2002. Mechanical strain and fluid movement both activate extracellular regulated kinase (ERK) in osteoblast-like cells but via different signaling pathways. *Bone*. 31:186–194. doi:10.1016/S8756-3282(02)00797-4

Karsenty, G., and E.F. Wagner. 2002. Reaching a genetic and molecular understanding of skeletal development. *Dev. Cell*. 2:389–406. doi:10.1016/S1534-5807(02)00157-0

Korbling, M., and Z. Estrov. 2003. Adult stem cells for tissue repair - a new therapeutic concept? *N. Engl. J. Med.* 349:570–582. doi:10.1056/NEJMra022361

Laing, A.J., J.P. Dillon, E.T. Condon, J.T. Street, J.H. Wang, A.J. McGuinness, and H.P. Redmond. 2007. Mobilization of endothelial precursor cells: Systemic vascular response to musculoskeletal trauma. *J. Orthop. Res.* 25:44–50. doi:10.1002/jor.20228

Li, Y., X. He, J. Schembri-King, S. Jakes, and J. Hayashi. 2000. Cloning and characterization of human Lnk, an adaptor protein with pleckstrin homology and Src homology 2 domains that can inhibit T cell activation. *J. Immunol.* 164:5199–5206.

Linden, M., A. Sirsjo, L. Lindbom, G. Nilsson, and A. Gidlof. 1995. Laser-Doppler perfusion imaging of microvascular blood flow in rabbit tenuissimus muscle. *Am. J. Physiol.* 269:H1496–H1500.

Liu, D., D.C. Genetos, Y. Shao, D.J. Geist, J. Li, H.Z. Ke, C.H. Turner, and R.L. Duncan. 2008. Activation of extracellular-signal regulated kinase (ERK1/2) by fluid shear is Ca(2+)- and ATP-dependent in MC3T3-E1 osteoblasts. *Bone*. 42:644–652. doi:10.1016/j.bone.2007.09.058

Manigrasso, M.B., and J.P. O'Connor. 2004. Characterization of a closed femur fracture model in mice. *J. Orthop. Trauma*. 18:687–695. doi:10.1097/00005131-200411000-00006

Marsh, D. 1998. Concepts of fracture union, delayed union, and nonunion. *Clin. Orthop. Relat. Res.*:S22–S30. doi:10.1097/00003086-199810001-00004

Matsumoto, T., A. Kawamoto, R. Kuroda, M. Ishikawa, Y. Mifune, H. Iwasaki, M. Miwa, M. Horii, S. Hayashi, A. Oyamada, et al. 2006. Therapeutic potential of vasculogenesis and osteogenesis promoted by peripheral blood CD34-positive cells for functional bone healing. *Am. J. Pathol.* 169:1440–1457. doi:10.2353/ajpath.2006.060064

Matsumoto, T., Y. Mifune, A. Kawamoto, R. Kuroda, T. Shoji, H. Iwasaki, T. Suzuki, A. Oyamada, M. Horii, A. Yokoyama, et al. 2008. Fracture induced mobilization and incorporation of bone marrow-derived endothelial progenitor cells for bone healing. *J. Cell. Physiol.* 215:234–242. doi:10.1002/jcp.21309

Mauch, P., C. Lamont, T.Y. Neben, C. Quinto, S.J. Goldman, and A. Witsell. 1995. Hematopoietic stem cells in the blood after stem cell factor and interleukin-11 administration: evidence for different mechanisms of mobilization. *Blood*. 86:4674–4680.

Nakamura, Y., F. Tajima, K. Ishiga, H. Yamazaki, M. Oshimura, G. Shiota, and Y. Murawaki. 2004. Soluble c-kit receptor mobilizes hematopoietic stem cells to peripheral blood in mice. *Exp. Hematol.* 32:390–396. doi:10.1016/j.exphem.2004.01.004

Nakazawa, T., A. Nakajima, N. Seki, A. Okawa, M. Kato, H. Moriya, N. Amizuka, T.A. Einhorn, and M. Yamazaki. 2004. Gene expression of periostin in the early stage of fracture healing detected by cDNA microarray analysis. *J. Orthop. Res.* 22:520–525. doi:10.1016/j.orthres.2003.10.007

Olmsted-Davis, E.A., Z. Gugala, F. Camargo, F.H. Gannon, K. Jackson, K.A. Kienstra, H.D. Shine, R.W. Lindsey, K.K. Hirschi, M.A. Goodell, et al. 2003. Primitive adult hematopoietic stem cells can function as osteoblast precursors. *Proc. Natl. Acad. Sci. USA*. 100:15877–15882. doi:10.1073/pnas.2632959100

Petite, H., V. Viateau, W. Bensaid, A. Meunier, C. de Pollak, M. Bourguignon, K. Oudina, L. Sedel, and G. Guillemin. 2000. Tissue-engineered bone regeneration. *Nat. Biotechnol.* 18:959–963 (see comment). doi:10.1038/79449

Rhee, S.T., L. El-Bassiony, and S.R. Buchman. 2006. Extracellular signal-related kinase and bone morphogenetic protein expression during distraction osteogenesis of the mandible: in vivo evidence of a mechanotransduction mechanism for differentiation and osteogenesis by mesenchymal precursor cells. *Plast. Reconstr. Surg.* 117:2243–2249. doi:10.1097/01.prs.0000224298.93486.1b

Rodriguez-Merchan, E.C., and F. Forriol. 2004. Nonunion: general principles and experimental data. *Clin. Orthop. Relat. Res.*:4–12. doi:10.1097/00003086-200402000-00003

Slack, J.M. 2000. Stem cells in epithelial tissues. *Science*. 287:1431–1433. doi:10.1126/science.287.5457.1431

Takahashi, T., C. Kalka, H. Masuda, D. Chen, M. Silver, M. Kearney, M. Magner, J.M. Isner, and T. Asahara. 1999. Ischemia- and cytokine-induced mobilization of bone marrow-derived endothelial progenitor cells for neovascularization. *Nat. Med.* 5:434–438. doi:10.1038/8462